INVESTIGATION OF THE ELECTRONIC STRUCTURE OF THE RUTHENIUM DYES USED IN SOLAR CELLS BY COMBINING HARTREE-FOCK THEORY WITH THE QUANTUM MONTE CARLO TECHNIQUE

A Thesis Submitted to
the Graduate School of Engineering and Sciences of
İzmir Institute of Technology
in Partial Fulfillment of the Requirements for the Degree of

MASTER OF SCIENCE

in Physics

by
Irmak Çağlar BERKMAN

December 2015
İZMİR

We approve the thesis of **Irmak Çağlar BERKMAN**

Examining Committee Members:

Prof. Dr. Nejat BULUT
Department of Physics, İzmir Institute of Technology

Prof. Dr. Ramazan Tuğrul SENGER
Department of Physics, İzmir Institute of Technology

Assoc. Prof. Dr. Ümit AKINCI
Department of Physics, Dokuz Eylul University

28 December 2015

Prof. Dr. Nejat BULUT
Supervisor, Department of Physics,
İzmir Institute of Technology

Prof. Dr. Nejat BULUT
Head of the Department of
Physics

Prof. Dr. Bilge KARAÇALI
Dean of the Graduate School of
Engineering and Sciences

ACKNOWLEDGMENTS

I would like to express the deepest appreciation to Professor Nejat BULUT for his great advise, patience and contributions for my study. His lectures on many body physics guided to me on my field.

I would like to thank my group mates Zafer KANDEMİR and Selma MAYDA for their great contributions for my study and guidence to me. Their friendship is very speacial to me.

Finally, I would like to express my gratitude to my family for their support and encouragement for my work.

The numerical calculations reported here were performed in part at the TUBITAK ULAKBIM, High Performance and Grid Computing Center (TRUBA resources). Financial support by the Turkish Scientific and Technical Research Council (TUBITAK grant number 113F242) is gratefully acknowledged.

ABSTRACT

INVESTIGATION OF THE ELECTRONIC STRUCTURE OF THE RUTHENIUM DYES USED IN SOLAR CELLS BY COMBINING HARTREE-FOCK THEORY WITH THE QUANTUM MONTE CARLO TECHNIQUE

The Haldane-Anderson model is constructed to describe the electronic properties of a system where a transition-metal impurity atom is added into a semiconductor host material. The electric and magnetic properties of the ruthenium-based dyes are investigated by using Haldane-Anderson model in this study. Because ruthenium-based dyes are semiconductor and ruthenium atom is a transition metal and its $4d$ orbitals are considered as impurities for dye molecules. Density Functional Theory (DFT) and Hartree-Fock Theory (HF) was used to obtain the Haldane-Anderson model parameters of the ruthenium-based dyes. Multi-orbital Hirsch-Fye Quantum Monte Carlo (HFQMC) algorithm was used to investigate effect of onsite Coulomb interactions of impurity 4d orbitals. Firstly, the Anderson model parameters are calculated by using Hartree-Fock and Density Functional Theory. After that, the occupation numbers of 4d orbitals and the all orbital occupancies of the dye molecules are obtained by using the Hirsch-Fye Quantum Monte Carlo algorithm and the magnetization of 4d orbitals are calculated. Finally, physical meaning of our results are discussed.

ÖZET

GÜNEŞ PİLLERİNDE KULLANILAN RUTHENİUM BOYALARIN ELEKTRONİK YAPISININ HARTREE FOCK KURAMI İLE KUANTUM MONTE CARLO TEKNİĞİNİN BİRLEŞTİRİLEREK İNCELENMESİ

Yarı-iletken ev sahibi malzemenin içine geçiş metali safsızlık atomu eklenerek oluşturulan bir sistemin elektronik özelliklerini incelemek için Haldane-Anderson modeli oluşturulmuştur. Bu çalışmada ruthenium-temelli boyaların elektronik ve manyetik özellikleri Haldane-Anderson modeli kullanılarak incelenmiştir. Çünkü, ruthenium-temelli boyalar yarı iletkendir ve ruthenium atomu bir geçiş metalidir ayrıca ruthenium atomunun $4d$ orbitalleri boya molekülü için safsızlık olarak kabul edilmiştir. Ruthenium-temelli boyaların Haldane-Anderson modeli parameterelerini elde etmek için Yoğunluk Fonksiyoneli Kuramı ve Hartree-Fock Kuramı kullanılmıştır. 4d orbitallerindeki Coulomb etkileşmelerinin sistemin elektronik özelliklerine etkisini incelemek için multi-orbital Hirsch-Fye Quantum Monte Carlo algoritması kullanılmıştır. İlk olarak, Hartree-Fock ve Yoğunluk Fonksiyoneli Kuramları kullanılarak Anderson modeli parametreleri hesaplanmıştır. Bundan sonra, Hirsch-Fye Kuantum Monte Carlo algoritması kullanılarak 4d orbitallerinin doluluk oranları, bütün sistemin doluluk oranları ve 4d orbitallerinin manyetizasyonları elde edilmiştir. Son olarak sonuçlarımızın fiziksel anlamları tartışılmıştır.

TABLE OF CONTENTS

LIST OF FIGURES

Figure **Page**

LIST OF TABLES

CHAPTER 1

INTRODUCTION

One of the most important thing for humanity is energy sources. Humankind is developing very fast and energy need of humanity is increasing rapidly. One of the solution of this energy need problem is solar energy. There are different kinds of solar energy cells to capture solar energy. Dye Sensitized Solar Cells (DSSC) is one of them. DSSC is a low-cost solar cell in the group of thin film solar cells [1]. Earlier version of DSSC based on semiconductor form between a photo-sensitized anode and an electrolyte and these are photoelectrochemical systems. The modern version of this type of solar cells known as Gratzel Cell and it was originally invented in 1988 by Brian O'Regan and Micheal Gratzel at UC Berkeley [2].

A modern DSSC is composed of a porous layer of titanium dioxide TiO_2 nanoparticles, covered with a molecular dye which absorb sunlight, like the chlorophyll in green leaves. When sunlight passes through the transparent electrode into the dye layer, it can excite electrons which flow into the TiO_2. The electrons flow toward the transparent electrode where they are collected for powering load. They are re-introduced into the cell on a metal electrode at the back, flowing into the electrolyte. In the electrolyte part, transported electrons go back into the dye molecules with red-ox reactions [3].

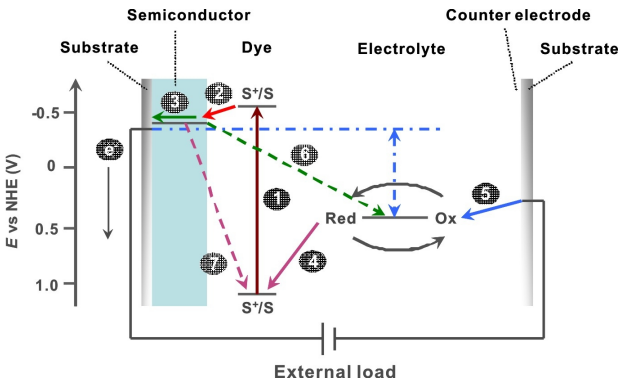

Figure 1.1. Working principle of dye sensitized solar cell (DSSC).

There is no efficient and also stable dye molecules in literature now and that is the main disadvantage of DSSC [4]. Different kinds of dye molecules have been produced in

the last 20 years. These dyes have organic and non-organic structures. We are going to investigate electronic structure of the ruthenium-based non-organic dyes and maybe this can help for finding new dye molecules in the future. We chose the ruthenium-based dyes because of their photochemical and physical properties. Ruthenium atom is a transition metal and ruthenium-based dyes are strongly correlated systems [5]. Ab-initio calculations (Density Functional Theory and Hartree-Fock Theory) have some problems to give correct results for strongly correlated system [6]. We are going to investigate this problem by using Haldane-Anderson impurity model [7]. Firstly, we will use DFT and HF theory with Gaussian 09 program and NBO package to find Anderson model parameters and then we will use HFQMC algorithm to find electronic properities of the Ruthenium-based dye molecules [8, 9].

Briefly, in Chapter 2, we investigated the molecular structure of the Ruthenium-based dyes and we explained why we chose N3, N719, N712 and Z907 dye molecules. Later, in Chapter 3 we decribed the basics of HF theory and DFT. In Chapter 4, we introduced the Anderson model and we decribed how we found the Anderson model parameters from the Fock matrix. In chapter 5, we showed HF theory, DFT, HF + QMC and DFT + QMC results and we compared Ab-initio calculations with the Quantum Monte Carlo calculations. Finally, in Appendix part, we gave detailed explanations for HF theory, DFT and HFQMC algorithm.

1.1. Molecular Structure of Ruthenium Dyes

Ruthenium-based dye molecules were first reported in 1991 by O'Regan and Gratzel in the Nature [1]. 7.1% efficiency was achieved by using these first ruthenium-based dyes. However, their molecular structures were complicated and the productions of them were difficult. Following dyes have different photochemical properties and we want to figure out the reasons of these differences. If we understand their electronic and magnetic properties correctly, we can then answer this question. We chose these following dyes for investigation of their electronic properties because N719 dye is the most efficent dye, Z907 dye is the most stable dye and N3 dye is the first one of these dyes and also molecular structure of N712 and N3 dyes are very similar to the N719 dye.

1.1.1. Molecular Structure of N3 Dye

In 1993, Nazeeruddin published DSSC with 10.3% efficiency [10], using N3 dye[cis-di(thiocyanato)bis(2,2-bipyridine-4,4-dicarboxylate)Ruthenium]. Molecular structure of N3 dye was much simpler than earlier version of dye molecules used in DSSC. Empirical formula of N3 dye is $[C_{26}H_{16}N_6O_8RuS_2]$ and ruthenium metal center atom instead of three like earlier versions.

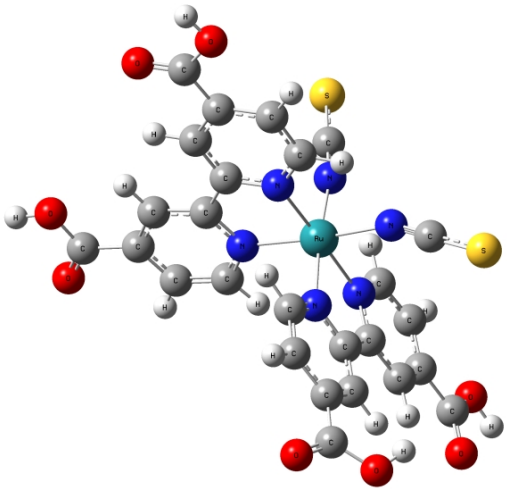

Figure 1.2. Atomic position of N3 Dye, with the empirical formula $[C_{26}H_{16}N_6O_8RuS_2]$. Nitrogen atoms are shown in dark blue, carbon in grey, ruthenium in light blue, hydrogen in white, oxygen in red and sulphur in yellow.

1.1.2. Molecular Structure of N719 Dye

In 2005, Nazeeruddin reported a new dye called N719. This new dye achieved 11.3% conversion efficiency in DSSC [11]. Molecular structure of N719 dye is similar to N3 dye with a empirical formula $[C_{26}H_{14}N_6O_8RuS_2]^{-2}$. N719 dye has two TBA^+(tetra butylamyn) and two H^+ counterions instead of four H^+ counterions in N3. When sunlight passes through to the DSSC, photons absorb by the dye molecules and they are excited from ground state to the excited state. Excited dye molecules adsorbed on the TiO_2 layer and they gives excited electrons into the conduction band of TiO_2 electrode.

When this process happening, dye molecules have different adsorption speed into the titanium dioxide layer. N3 dye and N719 dye have different adsorption speed onto the porous layer of TiO_2 electrode because they have different counterions and adsorption speed of N3 dye is 3 hours and adsorption speed of N719 dye is 24 hours. Consequence of speed difference of N719 dye gives better efficiency [3].

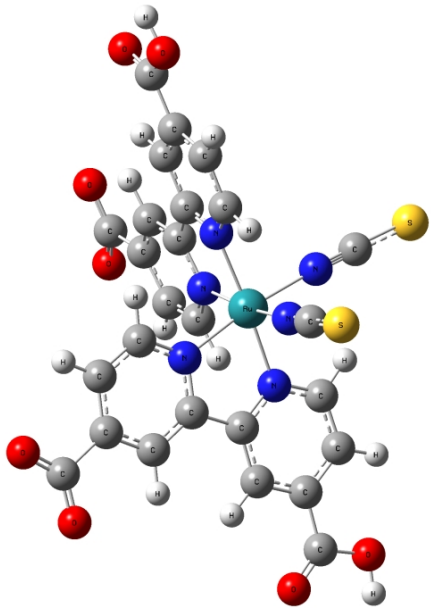

Figure 1.3. Atomic position of N719 Dye, with the empirical formula $[C_{26}H_{14}N_6O_8RuS_2]^{-2}$. Nitrogen atoms are shown in dark blue, carbon in grey, ruthenium in light blue, hydrogen in white, oxygen in red and sulphur in yellow. Molecular structures are taken from GaussView.

1.1.3. Molecular Structure of N712 Dye

N712 dye has four TBA^+ and no H^+ counterions. Molecular structure is similar to the N3 dye and the N719 dye except counterions part. Empirical formula of N712 Dye is $[C_{26}H_{12}N_6O_8RuS_2]^{-4}$. Adsorption speed on the porous layer of the TiO_2 is less than N719 dye (it takes much time then N719 dye to adsorbed on the TiO_2 layer). There is a certain value of adsorption speed for efficiency increase. Optimum value of adsorption time is around 24 hours. Because of these reasons, N712 dye has less efficienct then N719 dye [3]. However, we will investigate electronic structure of N712 dye because, we want to understand the effect of the counterion change.

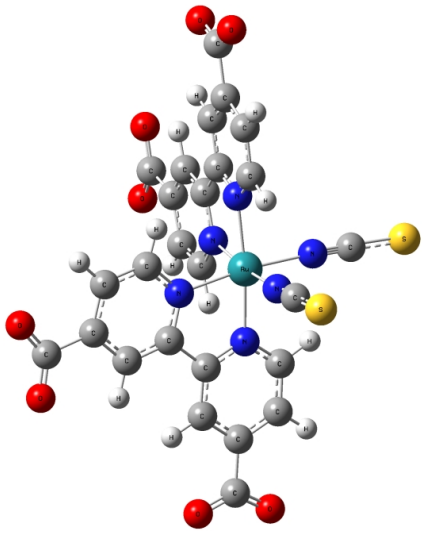

Figure 1.4. Atomic position of N712 Dye, with the empirical formula $[C_{26}H_{12}N_6O_8RuS_2]^{-4}$. Nitrogen atoms are shown in dark blue, carbon in grey, ruthenium in light blue, hydrogen in white, oxygen in red and sulphur in yellow. Molecular structures are taken from GaussView.

1.1.4. Molecular Structure of Z907 Dye

In 2003 Peng Wang $et\ al.$ reported Z907 Dye which is a stable quasi-solid-state amphiphilic ruthenium sensitizer with polymer gel electrolyte [12]. Emprical formula of Z907 Dye is $[C_{42}H_{52}N_6O_8RuS_2]$. It has some kind of similar molecular structure like N719 dye. Instead of TBA^+ counterions of N719 dye, it has C_9H_{19} molecules and wide band gap with TiO_2 up to $750nm$ and more stable than N719 dye. The DSSC with Z907 was sustained 1000h at 90^oC and it showed 94% of initial performance but Z907 dye is less efficient than N719 dye . This study was reported by [3, 12, 13].

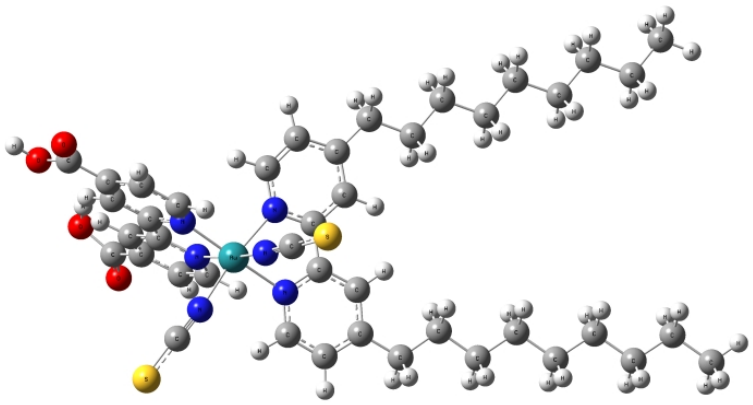

Figure 1.5. Atomic position of Z907 Dye, with the empirical formula $[C_{42}H_{52}N_6O_8RuS_2]$. Nitrogen atoms are shown in dark blue, carbon in grey, ruthenium in light blue, hydrogen in white, oxygen in red and sulphur in yellow. Molecular structures are taken from GaussView.

CHAPTER 2

HARTREE-FOCK AND DENSITY FUNCTIONAL THEORY

2.1. Hartree-Fock Theory

Investigation of many-body particles requires solving electronic Shrodinger equation and we need a trial wave function for solving electronic Shcrodinger eqution. True N-body ground state wave function can be approximated as linear combination of all possible Slater determinants [14, 15] because of the fermionic structure of the electrons of the system and Pauli's Exclusion Principle. Our method in this part of the study is Hartree-Fock approximation. This theory states that true N-body ground state wave function of the system can be approximated by a single Slater determinant which minimize the energy among all possible choice of all other single Slater determinants of the system. If we construct trial wave function from all possible Slater determinant, The trial wave function will define the system exactly but it is impossible to solve computationally [16–21]. We use Hartree-Fock theory because of this reason.

In Hartree-Fock theory, interactions between particles are approximated, either by neglecting all but taking the most important one or by taking all interactions into account in avarge fashion and consequently neglects the correlation between electrons [16–21].

In Hartree-Fock Theory, we are going to solve Fock matrix as eigenvalue equation (see appendix A for theoretical details) and it is as follows,

$$F_i\phi_i = \varepsilon_i\phi_i \tag{2.1}$$

Here F is the Fock operator, ϕ_i is canonical molecular orbital, and ε_i is eigenvalue of fock operator and Fock operator is defined as,

$$F_i = h_i + \sum_{ij}(J_{ij} - K_{ij}) \tag{2.2}$$

Where J_{ij} is coulomb operator and K_{ij} is exchange operator and they defined as,

$$J_{ij} =< \phi_i(1)\phi_j(2)|g_{12}|\phi_i(1)\phi_j(2) > \tag{2.3}$$

$$K_{ij} =< \phi_i(1)\phi_j(2)|g_{12}|\phi_j(1)\phi_i(2) > \tag{2.4}$$

here h_i is single particle operator,

$$h_i = -\frac{1}{2}{\nabla_i}^2 - \sum_a^{N_{nuclei}} \frac{Z_a}{|R_a - r_i|} \tag{2.5}$$

and two particle g_{ij}operator defined as,

$$g_{ij} = \frac{1}{|r_i - r_j|} \tag{2.6}$$

2.2. Density Functional Theory

The basis of (DFT) is the Hohenberg Kohn theorem [22]. DFT states that the ground state electronic energy can be completely determined by the electron density [16].

DFT is conceptually and computationally very similar to HF theory. We are taking account electron-electron correlation effects in DFT and we are neglecting this effects in Hartree-Fock Theory, because DFT can provide much better results when we compare with Hartree-Fock Theory.

Main goal in DFT, is to find exchange-correlation functional and also main problem of DFT is finding correct exchange-correlation functional. There are lots of different exchange-correlation functionals to describe electronic structure of the systems in literature. These different functionals can give good result or bad result depending on what we measure and what the electronic structure of the system is. Exchange-correlation functionals are constructed from theoretically and emprically and that is the reason why there are so much different functionals.

2.2.1. Hohenberg-Kohn Theory and Kohn-Sham Equation

There are two main ideas in the Hohenberg-Kohn theory. The first idea, electron density is a basic variable for determing system. The second idea, the ground state of the system can be found by using variational principle [16, 22]. (for details of theory see Appendix B) Hamiltonian of the many body system is

$$H_e = T_e + V_{ext} + V_{ee}. \tag{2.7}$$

Where T_e is the electronic kinetic energy, V_{ext} is interaction with the external potential energy and V_{ee} is the electron-electron interaction potential energy. General total energy can be written as

$$E[\rho] = F[\rho] + \int V_{ext}(r)\rho(r)dr. \tag{2.8}$$

Where V_{ext} is the interaction with nuclei and any other field and $F_{[}\rho]$ is defined as

$$F[\rho] = T[\rho] + V[\rho], \tag{2.9}$$

$$\tag{2.10}$$

$F[\rho]$ is independent of external potential but we don't know what it is and from Kohn-Sham theory [23] $F_{[\rho]}$ can be written as

$$F[\rho] = T_s[\rho] + \int \rho(r)\rho(r')drdr' + E_{xc}[\rho]. \tag{2.11}$$

where $T_s[\rho]$ is non interaction kinetic energy, $E_{xc}[\rho]$ is exchange-correlation energy and $J[\rho]$ is the Coulomb potential. Now we can write general energy expression for

DFT as follows

$$E_{DFT}[\rho] = T_s[\rho] + E_{ne}[\rho] + J[\rho] + E_{xc}[\rho]. \tag{2.12}$$

CHAPTER 3

ANDERSON MODEL FOR RUTHENIUM-BASED DYES

3.1. Anderson Model For Ruthenium-Based Dyes

Haldane-Anderson model describes the electronic structure of transition metal impurities in semiconductors[24]. Single-orbital Anderson Hamiltonian is [7]

$$\begin{aligned} H &= \sum_{k\sigma}(\varepsilon_k - \mu)\, {c_{k\sigma}}^{\dagger} c_{k\sigma} + \sum_{\sigma}(\varepsilon_d - \mu)\, d_\sigma^\dagger d_\sigma \\ &\quad + \sum_{k,\sigma}(V_k {c_{k\sigma}}^{\dagger} d_\sigma + h.c) + U n_{d\uparrow} n_{d\downarrow}. \end{aligned} \tag{3.1}$$

Where, ε_k denotes the eigenvalues of host electrons, $c_{k\sigma}$ is the destruction operator, ${c_{k\sigma}}^{\dagger}$ is the creation operator for host electrons, ε_d denotes the eigenvalues of the impuritiy electrons, V_k is the hybridization term between host and impurity electrons, U is the on site Coulomb interaction of d electrons, $n_{d\sigma}$ is the site occupation number of d electron with $\sigma = \uparrow$ and $\sigma = \downarrow$ which denotes up spin and down spin of electrons.

In this work we are interested to find electronic structure of Ruthenium based dyes. Ru atom is transition metal. Transition metals have partially filled d and f orbitals. Because of that we need to construct multi-orbital Anderson model [25]. Multi-orbital Anderson Hamiltonian is

$$\begin{aligned} H &= \sum_{m\,\sigma}(\varepsilon_m - \mu)\, c_{m\,\sigma}^\dagger\, c_{m\,\sigma} + \sum_{m\,\sigma}\sum_{\nu=1}^{5}(V_{m\,\nu}\, c_{m\,\sigma}^\dagger\, d_{\nu\,\sigma} + h.c.) \\ &\quad + \sum_{\nu=1}^{5}\sum_{\sigma}(\varepsilon_\nu - \mu)\, n_{\nu\,\sigma} + \sum_{\nu=1}^{5} U_\nu\, n_{\nu\uparrow}\, n_{\nu\downarrow}. \end{aligned}$$

In the single-orbital case $\vec{k}$ denotes the wave vector of the host lattice structure. However, in our work, we use the notation m for the discrete host eigenstates, ν is the

index of d orbitals ranging from 1 to 5 for Anderson model. Therefore, each molecular orbital can be expressed as

$$|\psi_n\rangle = \sum_{\nu=1}^{5} \beta_{n\nu}|d_\nu\rangle + \sum_{i=1}^{N-5} \beta_{ni}|\phi_i\rangle \tag{3.2}$$

where β_{nm} are the molecular orbital coefficients, $|d_\nu\rangle$ is the orthogonal atomic orbital of impurity, and $|\phi_i\rangle$ is the orthogonal atomic orbital of host. In Eq.(3.2), n is an index for the molecular wavefunctions, N represents the number of the basis functions, ν is an indec for only $4d$ orbitals of ruthenium atom and i an index for the rest of the atomic orbitals (host index).

In this work, we're going to use HF and DFT to find Anderson model parameters. After that, we will use these parameters in our QMC calculations and effect of the Coulomb repulsion between 4d orbitals are included in these results.

There is a lack of knowledge for understanding strongly corralated systems in pure DFT. We are taking into account electron-electron correlation effect in DFT calculations. On the other hand, in the pure HF theory, there is no correlation effect of electrons and Coulomb repulsion is taken in the mean field fashion.

3.2. Finding Anderson Model Parameters with Hartree-Fock and Density Functional Theory from Fock Matrix

To find the Anderson model parameters, our approach is getting Fock matrix by using the Gaussian 09 program with the NBO package [8, 9]. We use the NBO package since there is an option to get Fock matrix in orthogonal basis called Natural Atomic Orbitals (NAO). In the input file "FNAO" keyword gives us the Fock matrix in NAO basis. After getting Fock matrix, we divided it into two submatrices which are host part and impurity part [26].

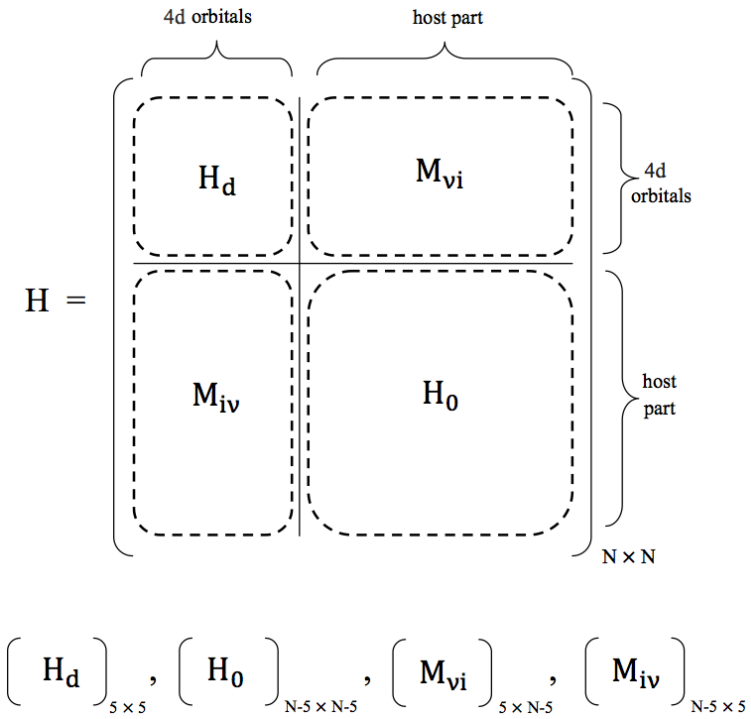

Figure 3.1. The Hamiltonian of the Fock matrix in the NAO basis (FNAO). We divided Fock matrix into the three parts. The $\mathrm{H_d}$ part contains the diagonal terms $\varepsilon_{d\nu}$ (effective energies of the $4d$ orbitals) and the off-diagonal terms $t_{\nu\nu'}$ (the hopping energies of the $4d$ orbitals). The $\mathrm{H_0}$ matrix represents the host Hamiltonian. $\mathrm{M_{\nu i}}$ and $\mathrm{M_{i\nu}}$ are the interacting terms between the impurity ($4d$ orbitals of ruthenium atom) and the host part.

The impurity part contains diagonal $\varepsilon_{d\nu}$ effective energy of 4d orbitals part and the nondiagonal $t_{\nu\nu'}$ hopping term between 4d orbitals part. H_0 is the host part, $\mathrm{M_{\nu i}}$ and $\mathrm{M_{i\nu}}$ are the interacting terms between the impurity and the host part.

We diagonalize the host part of Fock matrix by multiplying with f_{im} matrix and we also have to multiply interaction terms between the impurity and host part of the Fock matrix $\mathrm{M_{\nu i}}$ with f_{im} . If we define $V_{m\nu}$ as the new interaction term between host and impurity part as following [26],

$$V_{\nu m} = \sum_{i}^{N-5} M_{\nu i} f_{im} \ . \tag{3.3}$$

New Hamiltonian is

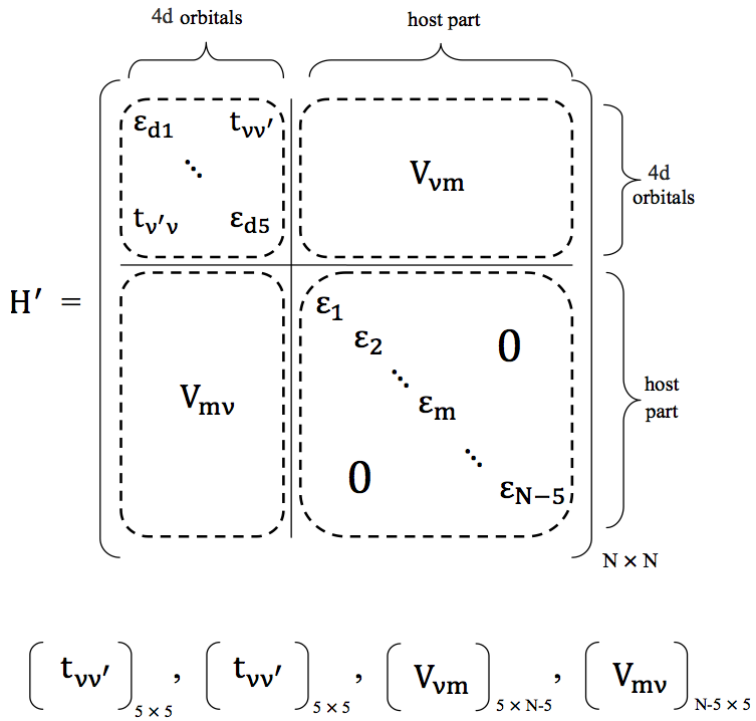

Figure 3.2. New Hamiltonian H' after diagonalization. The first part contains the diagonal terms $\varepsilon_{d\nu}$ (energies of the $4d$ orbitals) and the off-diagonal terms $t_{\nu\nu'}$ (hopping energies of the $4d$ orbitals). The host part contains ε_m the eigenvalues of the host Hamiltonian after diagonalization. $\mathrm{V}_{\nu\mathrm{m}}$ and $\mathrm{V}_{\mathrm{m}\nu}$ are the hybridization matrix elements between the impurity ($4d$ orbitals of ruthenium atom) and the host part.

We can find all Anderson Hamiltonian parameters from reading these matrix elements.

CHAPTER 4

QUANTUM MONTE CARLO MEASUREMENTS

4.1. Quantum Monte Carlo Measurements

Multi-orbital Hirsch-Fye quantum Monte Carlo technique [25](see Appendix C for details) allows us to find the numerical results of Green's functions of 4d orbitals. Firstly, we define the Green functions of 4d orbitals as following,

$$G_{\nu\,\nu'\,\sigma}(\tau) = -\left\langle T_\tau\, d_{\nu\,\sigma}(\tau'+\tau)\, d^\dagger_{\nu'\,\sigma}(\tau')\right\rangle, \tag{4.1}$$

$$\tag{4.2}$$

in Matsubara frequiencies. Here, subscript ν and ν' shows 4d orbitals of ruthenium atom, T_τ is the Matsubara time ordering operator and σ is the spin. d_ν and d'_ν obey the fermionic anti commutation relation:

$$\left\{\, d_\nu\,, d^\dagger_{\nu'}\,\right\} = \delta_{\nu,\nu'}. \tag{4.3}$$

Our primary goal in this work is to find the occupation number and the magnetization of 4d orbitals of ruthenium atom and the definition of occupation number and magnetization are;

$$M^z_\nu = d^\dagger_{\nu\uparrow}\, d_{\nu\uparrow} \,-\, d^\dagger_{\nu\downarrow}\, d_{\nu\downarrow}, \tag{4.4}$$

$$n_\nu = d^\dagger_{\nu\uparrow}\, d_{\nu\uparrow} \,+\, d^\dagger_{\nu\downarrow}\, d_{\nu\downarrow}. \tag{4.5}$$

With these definitions, we can find the static QMC measurements and these static

measurements are equal time measurements. In chapter 6, we will investigate the occupation number of the 4d orbitals of ruthenium atom $< n_\nu >$ and the equal-time magnetic correlation function of between 4d orbitals of ruthenium atom $< (M_\nu^z)^2 >$.

4.1.1. Static Quantum Monte Carlo Measurements

In our simulations warm up sweeps describe the thermalization of the system at given temperature. During the warm up sweeps, Hubbard Stratonovich spins (see Appendic C) flip via random number ratio and system can be arranged realisticly depending on the number of sweeps. We can find avarage values and error values of our calculations by using standart deviation. If we increase the number of warm up sweeps, this will minimize our errors but it will increase the computing time. Therefore, we calibrated number of warm up sweeps and measurements sweeps. In the warm up sweeps section, there are no any measurements made. After the warm up sweeps part, measurements strart.

By using fermionic anti commutation relation of $d_{\nu\uparrow}^\dagger$ and $d_{\nu\uparrow}$, the definitions of the Green's function and Wick's Theorem, we will calculate the occupation number of 4d orbitals, magnetic moment of 4d orbitals.

The occupation number of 4d orbitals,

$$\begin{aligned} \langle\, n_\nu \,\rangle &= \left\langle\, d_{\nu\uparrow}^\dagger\, d_{\nu\uparrow} \,+\, d_{\nu\downarrow}^\dagger\, d_{\nu\downarrow} \,\right\rangle \\ &= \frac{1}{L} \sum_{i=1}^{L} \langle\, [\,(\,1 \,-\, G_{\nu\,\nu\uparrow}(\tau_i,\tau_i)\,) \,+\, (\,1 \,-\, G_{\nu\,\nu\downarrow}(\tau_i,\tau_i)\,)\,] \rangle_{\{S_{l\nu}\}}\,. \end{aligned} \tag{4.6}$$

Square of the magnetic moment of 4d electrons,

$$
\begin{aligned}
\langle\, (M_\nu^z)^2 \,\rangle &= \left\langle \left(d_{\nu\uparrow}^\dagger\, d_{\nu\uparrow} - d_{\nu\downarrow}^\dagger\, d_{\nu\downarrow} \right) \left(d_{\nu\uparrow}^\dagger\, d_{\nu\uparrow} - d_{\nu\downarrow}^\dagger\, d_{\nu\downarrow} \right) \right\rangle \\
&= \left\langle \left(d_{\nu\uparrow}^\dagger\, d_{\nu\uparrow} - d_{\nu\downarrow}^\dagger\, d_{\nu\downarrow} \right) \left(d_{\nu\uparrow}^\dagger\, d_{\nu\uparrow} - d_{\nu\downarrow}^\dagger\, d_{\nu\downarrow} \right) \right\rangle \\
&\quad + \left\langle \left(d_{\nu\uparrow}\, d_{\nu\uparrow}^\dagger\, d_{\nu\uparrow}^\dagger\, d_{\nu\uparrow} + d_{\nu\downarrow}\, d_{\nu\downarrow}^\dagger\, d_{\nu\downarrow}^\dagger\, d_{\nu\downarrow} \right) \right\rangle \\
&= \frac{1}{L} \sum_{i=1}^{L} \left\langle \left[\left(G_{\nu\,\nu\uparrow}(\tau_i,\tau_i) - G_{\nu\,\nu\downarrow}(\tau_i,\tau_i) \right)^2 \right.\right. \\
&\quad + G_{\nu\,\nu\uparrow}(\tau_i,\tau_i)\, \left(1 - G_{\nu\,\nu\uparrow}(\tau_i,\tau_i) \right) \\
&\quad \left.\left. + G_{\nu\,\nu\downarrow}(\tau_i,\tau_i)\, \left(1 - G_{\nu\,\nu\downarrow}(\tau_i,\tau_i) \right) \right] \right\rangle_{\{S_{l\nu}\}} . \qquad (4.7)
\end{aligned}
$$

$\{S_{l\nu}\}$ denotes the Hubbard-Stratonovich field summation.

4.2. Double Counting Correction

In our calculations, it is important to note that the onsite Coulomb interaction U is taken into account twice, first in Ab-inito calculation (HF and DFT) and second in the QMC calculations. We need to extract double counting term from the energy levels of the 4d orbitals of ruthenium atom called $\varepsilon_{d\nu}$. We used double counting definition from [27]. Our new energy levels of 4d orbitals are $\tilde{\varepsilon}_{d\nu}$ as the following,

$$
\tilde{\varepsilon}_{d\nu} = \varepsilon_{d\nu} - \mu_{dc} \qquad (4.8)
$$

Here, μ_{dc} is the double counting term and we can describe as the following,

$$
\mu_{dc} = \frac{U < n_{dc}^{HF} >}{10} \qquad (4.9)
$$

where $< n_{dc}^{HF} >$ is the average electron number of 4d orbitals of ruthenium atom which is obtained by HF theory and U is the on-site Coulomb interaction term.

We use the same relation for DFT only difference here is $< n_{dc}^{DFT} >$ the average

electron number of 4d orbitals of ruthenium atom which is obtained by DFT.

$$\mu_{dc} = \frac{U < n_{dc}^{DFT} >}{10} \tag{4.10}$$

CHAPTER 5

RESULTS

5.1. Hartree-Fock Results

We define density of states(DOS) $D(\varepsilon)$ for $4d$ orbitals of ruthenium atom plus host states as follows,

$$\begin{aligned} D(\varepsilon) &= \sum_{n=1}^{N} \delta(\varepsilon - E_n)) \\ &= \sum_{n=1}^{N} \frac{\gamma/\pi}{\gamma^2 + (\varepsilon - E_n)^2} \end{aligned} \tag{5.1}$$

Here E_n are the eigenvalues of the Fock operator and N is the total basis function. We define DOS $D_0(\varepsilon)$ of host states as follows,

$$\begin{aligned} D_0(\varepsilon) &= \sum_{n=1}^{N} \delta(\varepsilon - \varepsilon_m)) \\ &= \sum_{n=1}^{N} \frac{\gamma/\pi}{\gamma^2 + (\varepsilon - \varepsilon_m)^2} \end{aligned} \tag{5.2}$$

Here ε_m are the energy levels of the host states and we use here $N - 5$ basis function because we want to find DOS without $4d$ orbitals of ruthenium atom. γ is broadness factor and we plotted DOS graph for different γ values 0.1 and 0.2.

5.1.1. Computational Details

HF theory results of ruthenium-based dyes (N3, N719, N712 and Z907) are calculated by using Gaussian 09 program [8] with NBO package [9]. Molecular geometry is obtained by using GaussView [28] which is visualization program of molecular sturcture of the systems. In these calculation, atomic coordinates of optimized structure of N3 dye taken from [29], atomic coordinates of optimized structure of N719 dye taken from [29], atomic coordinates of optimized structure of N712 dye taken from [29] and Z907 dye constructed from N719 dye with the information from [30] after that, all dyes are optimized by using Gaussian 09 program with B3LYP (Becke-three-LeeYangParr hybrid functional) [31–34] functional. After finding optimized structure of all ruthenium-based dyes we did Hartree-Fock calculation with LANL2DZ basis set for Ru atom and 6-31G(d) basis set for the rest of the atoms (C, H, O, N, S). For the transition metal Ru atom, the effective core potential basis set LANL2DZ (Los Alamos ECP plus double zeta) is used [35–38].

5.1.2. Measurement of N719

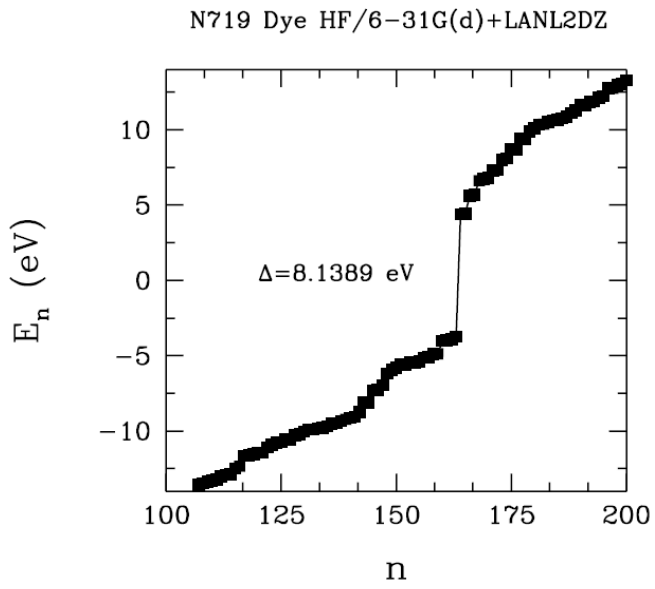

Figure 5.1. Energy eigenvalues E_n versus n for N719 dye is plotted. The forbidden energy gap (Δ) is approximately 8.14 eV between HOMO and LUMO levels. Here, n is the number of basis functions;$n = 1, 2, ..., N$.

4d orbitals	ε_{dv} **(eV)**	$\langle n_v \rangle$
xz	-3.66265	1.63283
3z²-r²	-3.24360	1.59633
x²-y²	-2.64223	1.50150
xy	-1.27621	1.32799
yz	2.57420	0.84509

Table 5.1. Occupation number and energy level of 4d orbitals of N719 dye

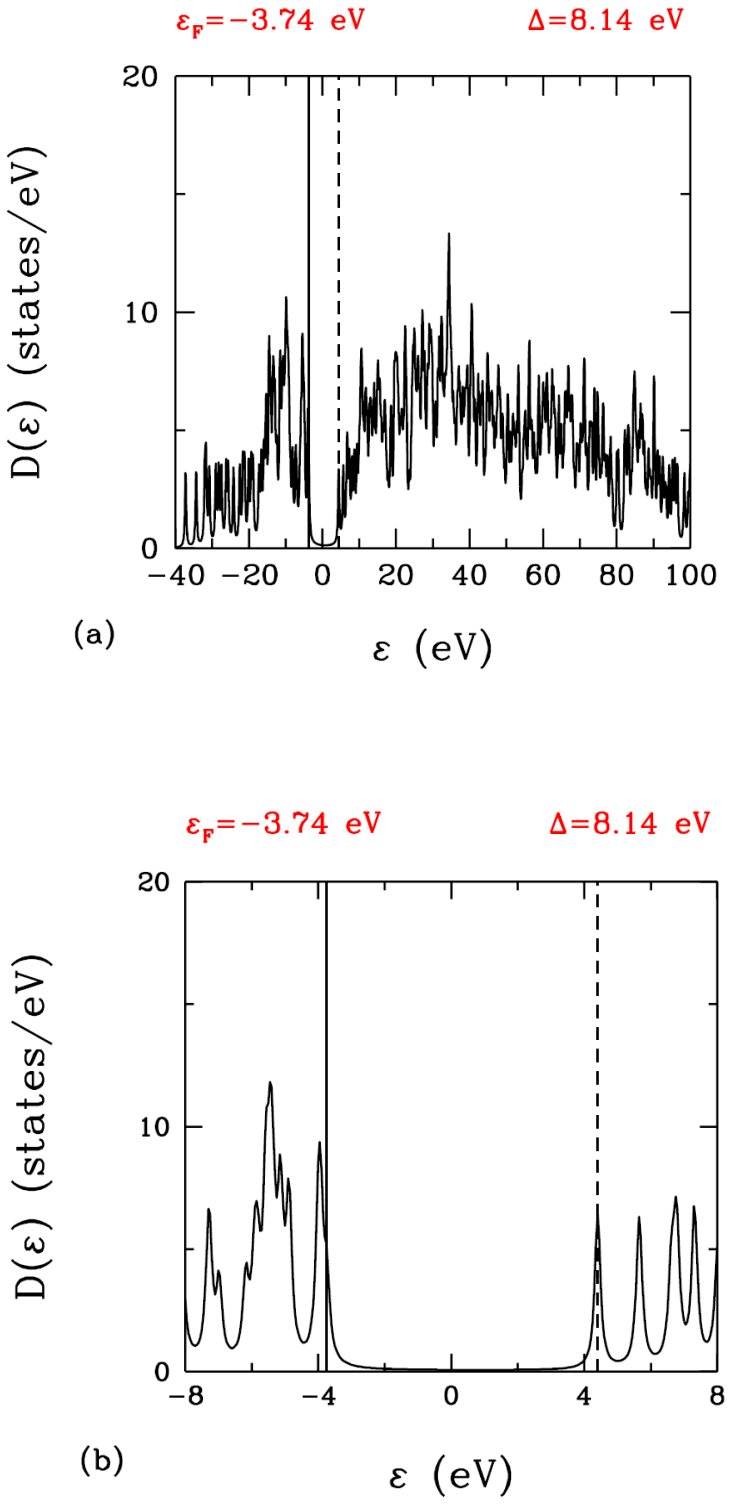

Figure 5.2. For all orbitals density of states $D(\varepsilon)$ versus ε are calculated by using eq. 5.1 (a) The calculated density of state (DOS) of N719 Dye is plotted for $\gamma = 0.2$. (b) This figure is plotted for $\gamma = 0.1$ with the range -8 to 8.

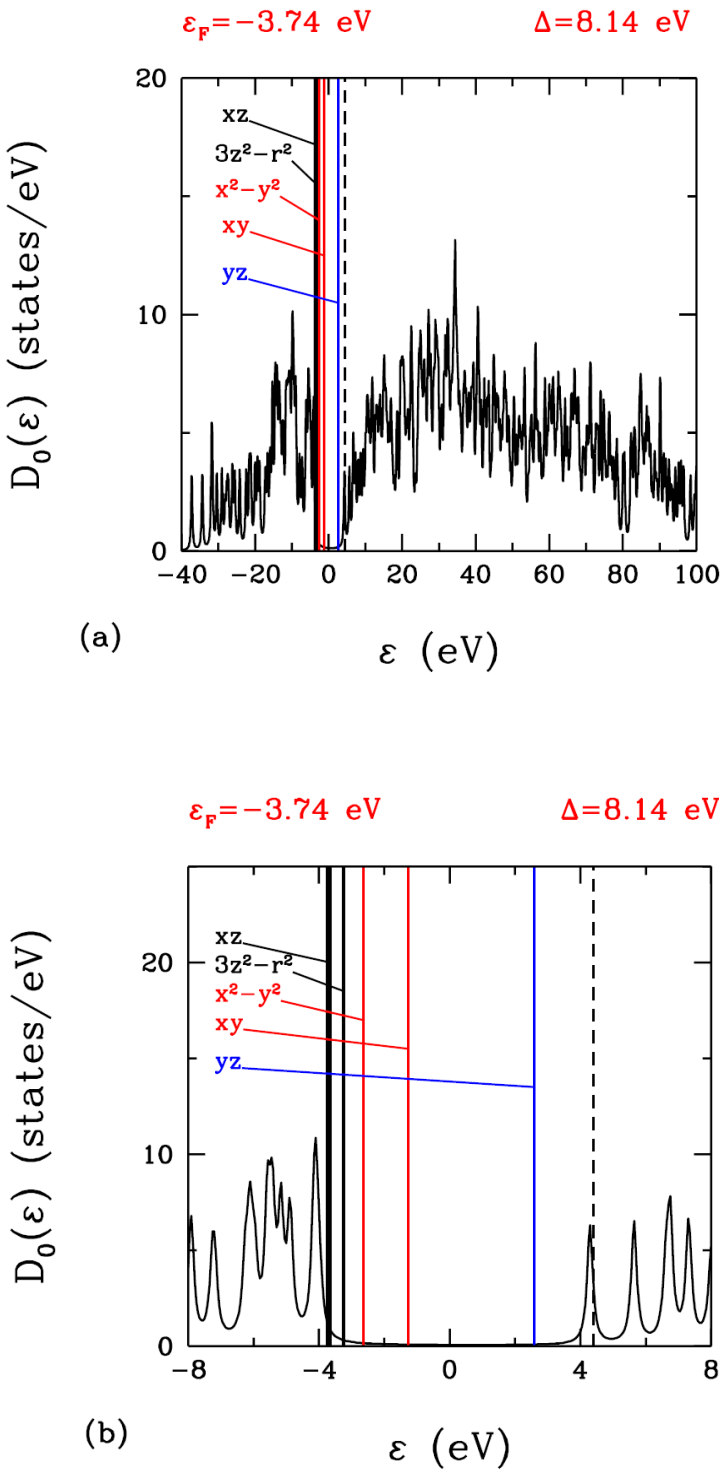

Figure 5.3. Without $4d$ orbitals density of states $D(\varepsilon)$ versus ε are calculated by using eq. 5.2 (a) The calculated density of state (DOS) of N719 Dye without the $4d$ is plotted for $\gamma = 0.2$. The coloured vertical lines represent the position of $4d$ orbitals. (b) This figure is plotted for $\gamma = 0.1$ with the range -8 to 8 .

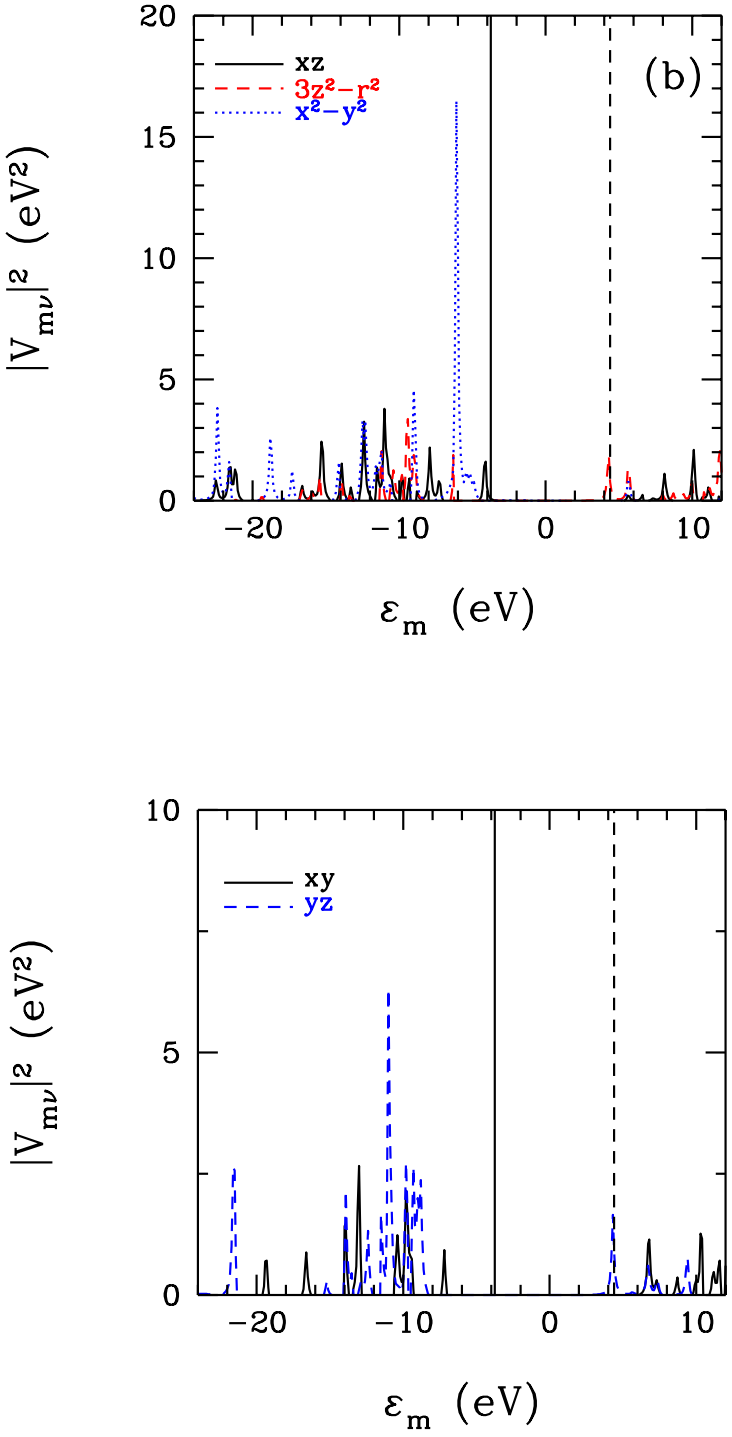

Figure 5.4. Square of the hybridization matrix elements $V_{m\nu}$ between the host states and the $Ru(4d_\nu)$ states plotted as a function of the energy of the host states, ε_m. Here, the vertical solid and dashed lines denote the HOMO and LUMO levels.

5.2. DFT Results

We define density of states(DOS) $D(\varepsilon)$ for $4d$ orbitals of ruthenium atom plus host states as follows,

$$\begin{aligned} D(\varepsilon) &= \sum_{n=1}^{N} \delta(\varepsilon - E_n)) \\ &= \sum_{n=1}^{N} \frac{\gamma/\pi}{\gamma^2 + (\varepsilon - E_n)^2} \end{aligned} \tag{5.3}$$

Here E_n are the eigenvalues of the Fock operator and N is the total basis function. We define DOS $D_0(\varepsilon)$ of host states as follows,

$$\begin{aligned} D_0(\varepsilon) &= \sum_{n=1}^{N} \delta(\varepsilon - \varepsilon_m)) \\ &= \sum_{n=1}^{N} \frac{\gamma/\pi}{\gamma^2 + (\varepsilon - \varepsilon_m)^2} \end{aligned} \tag{5.4}$$

Here ε_m are the energy levels of the host states and we use here $N - 5$ basis function because we want to find DOS without $4d$ orbitals of ruthenium atom. γ is broadness factor and we plotted DOS graph for different γ values 0.1 and 0.2.

5.2.1. Computational Details

DFT results of ruthenium-based Dyes (N3, N719, N712 and Z907) are calculated by using Gaussian 09 program [8] with NBO package [9]. Molecular geometry is obtained by using GaussView [28] which is visualization program of molecular sturcture of the systems. In these calculation, atomic coordinates of optimized structure of N3 taken from [29], atomic coordinates of optimized structure of N719 dye taken from [29], atomic coordinates of optimized structure of N712 dye taken from [29] and Z907 dye constructed from N719 dye with the information from [30] after that all dyes are optimized by using Gaussian 09 program with B3LYP (Becke-three-LeeYangParr hybrid functional) [31–34]

functional. After finding optimized structure of all ruthenium-based dyes we did DFT calculation also we used B3LYP hybrid functional with LANL2DZ basis set for Ru atom and 6-31G(d) basis set for the rest of the atoms (C, H, O, N, S). For the transition metal Ru atom, the effective core potential basis set LANL2DZ (Los Alamos ECP plus double zeta) is used [35–38].

5.2.2. Measurement of N719

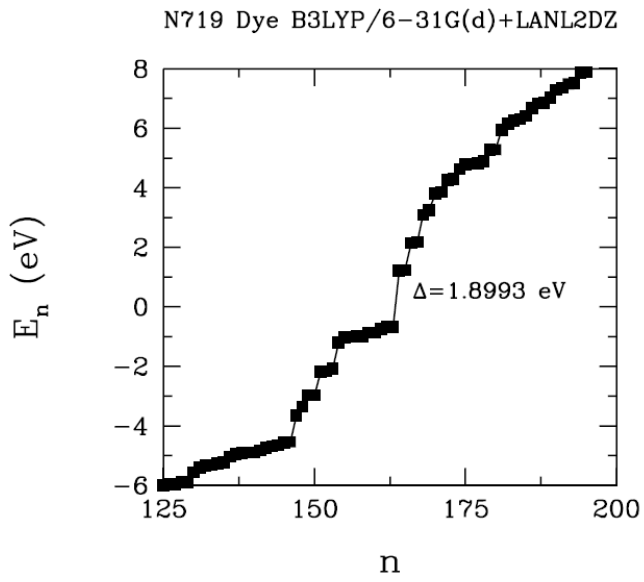

Figure 5.5. Energy eigenvalues E_n versus n for N719 dye is plotted. The forbidden energy gap (Δ) is approximately 1.90 eV between HOMO and LUMO bands. Here, n is the number of basis functions;$n = 1, 2, ..., N$.

4d orbitals	ε_{dv} **(eV)**	$\langle n_v \rangle$
xz	-1.65717	1.59698
x^2-y^2	-1.51840	1.53774
$3z^2$-r^2	-1.45581	1.59379
xy	-1.23540	1.35743
yz	-0.71566	1.01547

Table 5.2. Occupation number and energy level of 4d orbitals of N719 dye

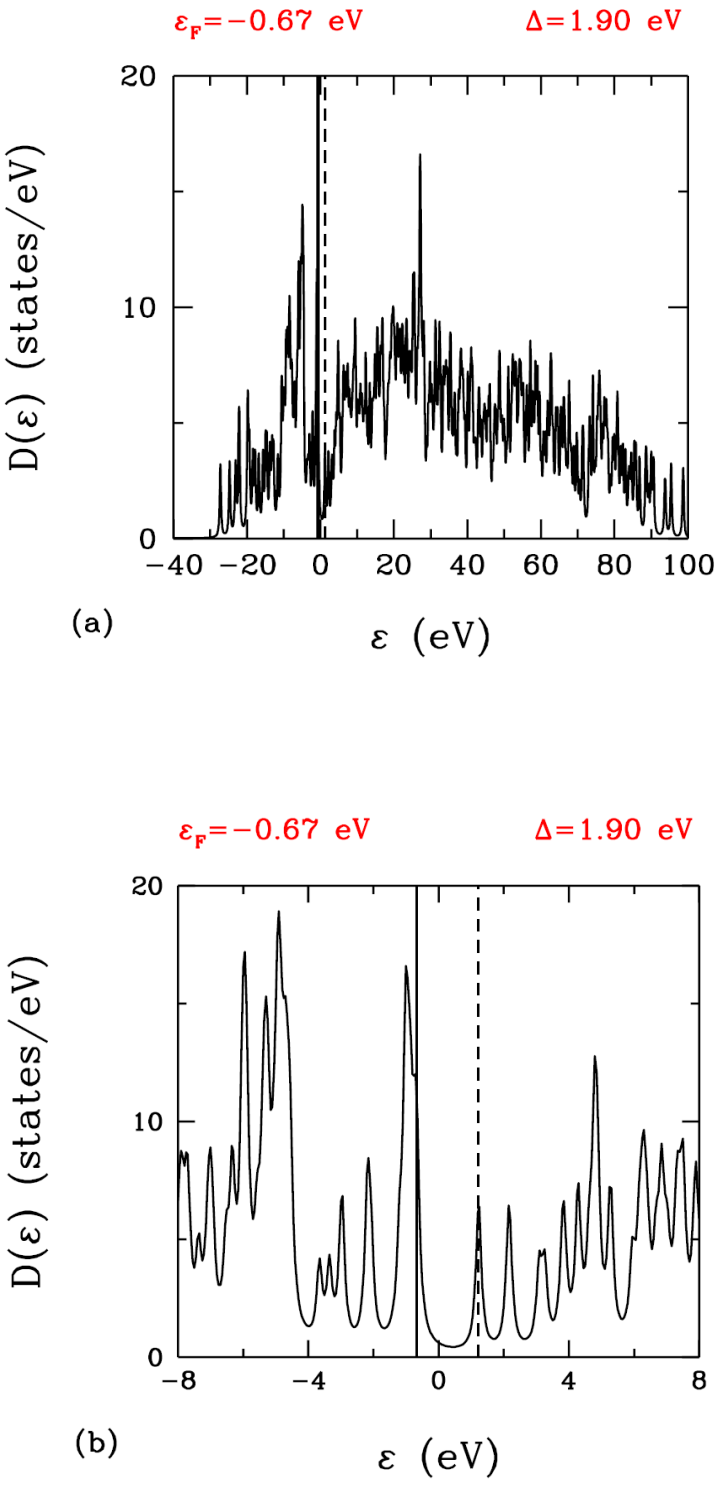

Figure 5.6. For all orbitals density of states $D(\varepsilon)$ versus ε are calculated by using eq. 5.3 (a) The calculated density of state (DOS) of N719 Dye is plotted for $\gamma = 0.2$. (b) This figure is plotted for $\gamma = 0.1$ with the range -8 to 8.

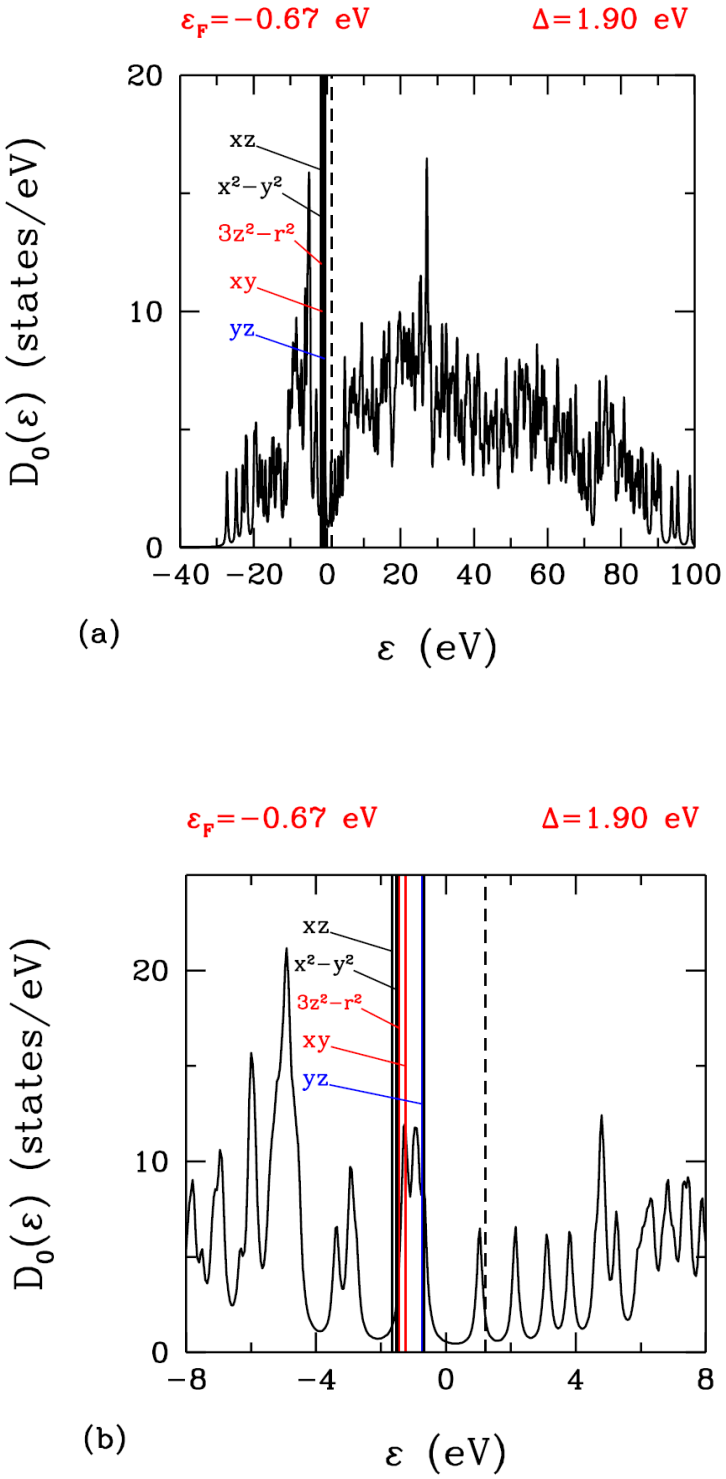

Figure 5.7. Without $4d$ orbitals density of states $D(\varepsilon)$ versus ε are calculated by using eq. 5.4 (a) The calculated density of state (DOS) of N719 Dye without the $4d$ is plotted for $\gamma = 0.2$. The coloured vertical lines represent the position of $4d$ orbitals. (b) This figure is plotted for $\gamma = 0.1$ with the range -8 to 8.

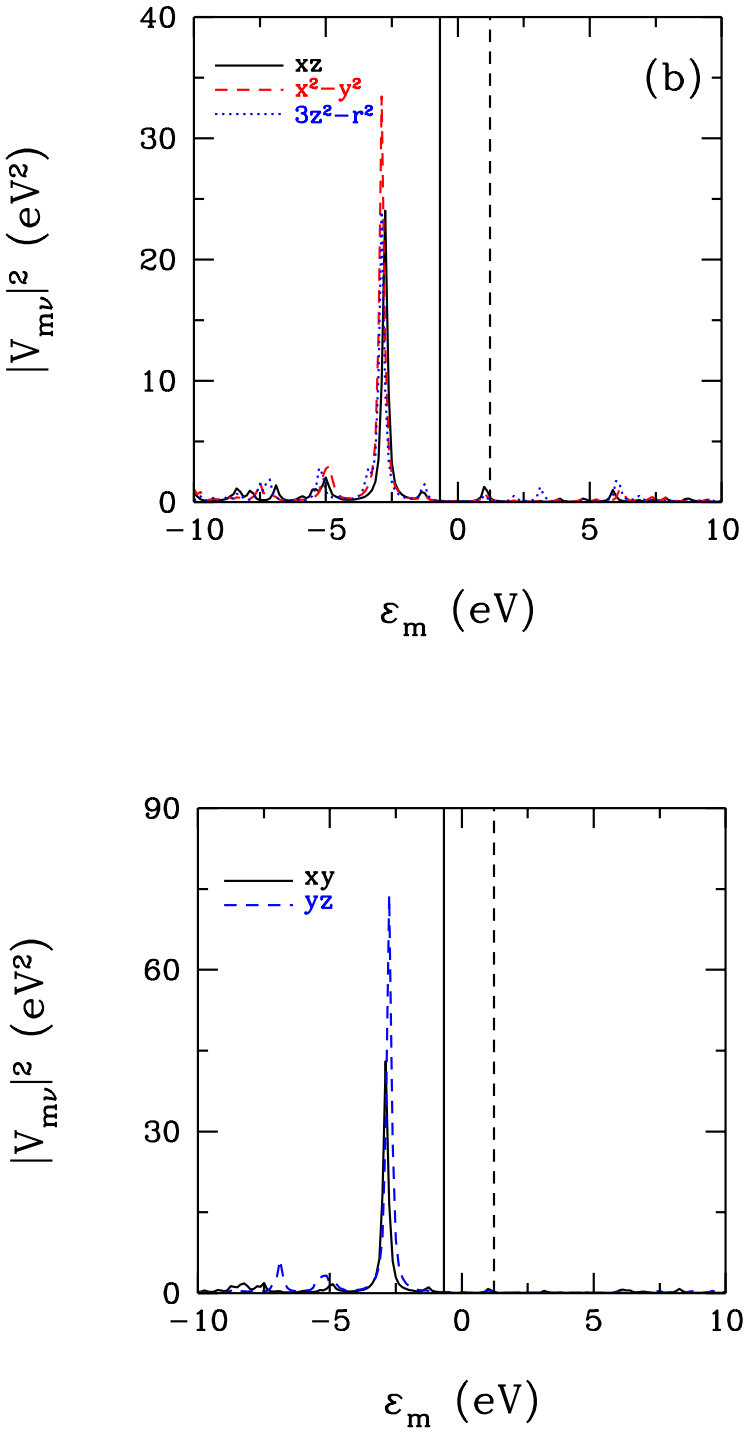

Figure 5.8. Square of the hybridization matrix elements $V_{m\nu}$ between the host states and the $Ru(4d_\nu)$ states plotted as a function of the energy of the host states, ε_m. Here, the vertical solid and dashed lines denote the HOMO and LUMO levels, respectively.

5.3. QMC Results of N719

Solving Anderson Hamiltonian is very difficult numerically and of the Coulomb repulsion of the $(4d_\nu)$ orbitals of ruthenium atom. Therefore, we used Hirsch-Fye Quantum Monte Carlo (HFQMC) algortihm (for details see appendix C) [39] which takes account strong Coulomb repulsion effects without any approximation.

We did static Quantum Monte Carlo calculations by using HFQMC algortihm and we found occupation number of $(4d_\nu)$ orbitals of the ruthenium atom, occupation number of host states of the N719 dye and total electron number of N719 dye, square of local magnetic moment of $(4d_\nu)$ orbitals of the ruthenium atom.

5.3.1. Hartree-Fock + QMC Results

We found Anderson Hamiltonian parameter from Hartree-Fock Theory for QMC calculations in this section. We found occupation number of host states of the N719 dye and occupation number of $(4d_\nu)$ orbitals of the ruthenium atom for temperature 1000K. In these calculations $\beta = \Delta\tau L$ are parameters of Hirsch-Fye algortihm and these values are $\Delta\tau = 0.3625$ and $L = 32$. Also we found square of local magnetic moment of $(4d_\nu)$ orbitals of ruthenium atom for $T = 1000K$. For magnetic moment calculations Hirsch-Fye parameters values are $\Delta\tau = 0.3625$ and $L = 32$. For all calculations number of warm up sweeps are 1000 and number of measurement sweeps are 1000.

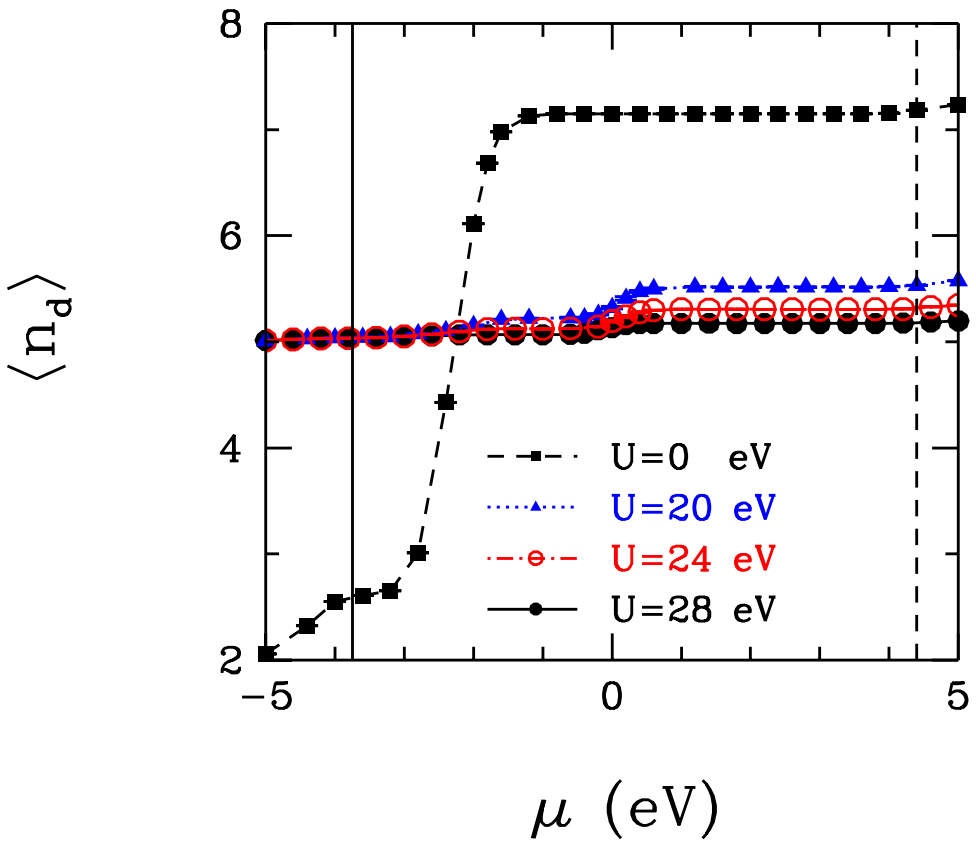

Figure 5.9. Occupation number of the $(4d_\nu)$ orbitals of the ruthenium atom $\langle\, n_d \,\rangle$ as a function of the chemical potential μ. Here, results are shown for different values of the onsite Coulomb repulsion U. In addition, the vertical solid and dashed lines denote the HOMO and LUMO levels, respectively.

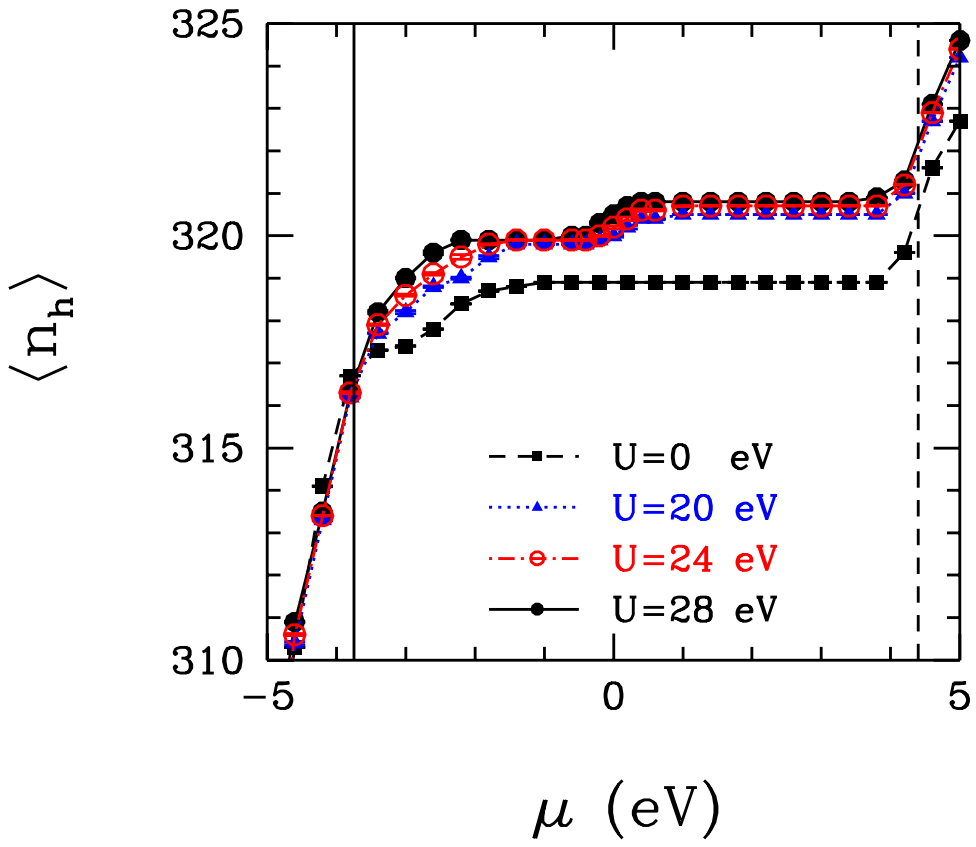

Figure 5.10. Occupation number of the host states of N719 dye $\langle n_h \rangle$ as a function of the chemical potential μ. Here, results are shown for different values of the onsite Coulomb repulsion U. In addition, the vertical solid and dashed lines denote the HOMO and LUMO levels, respectively.

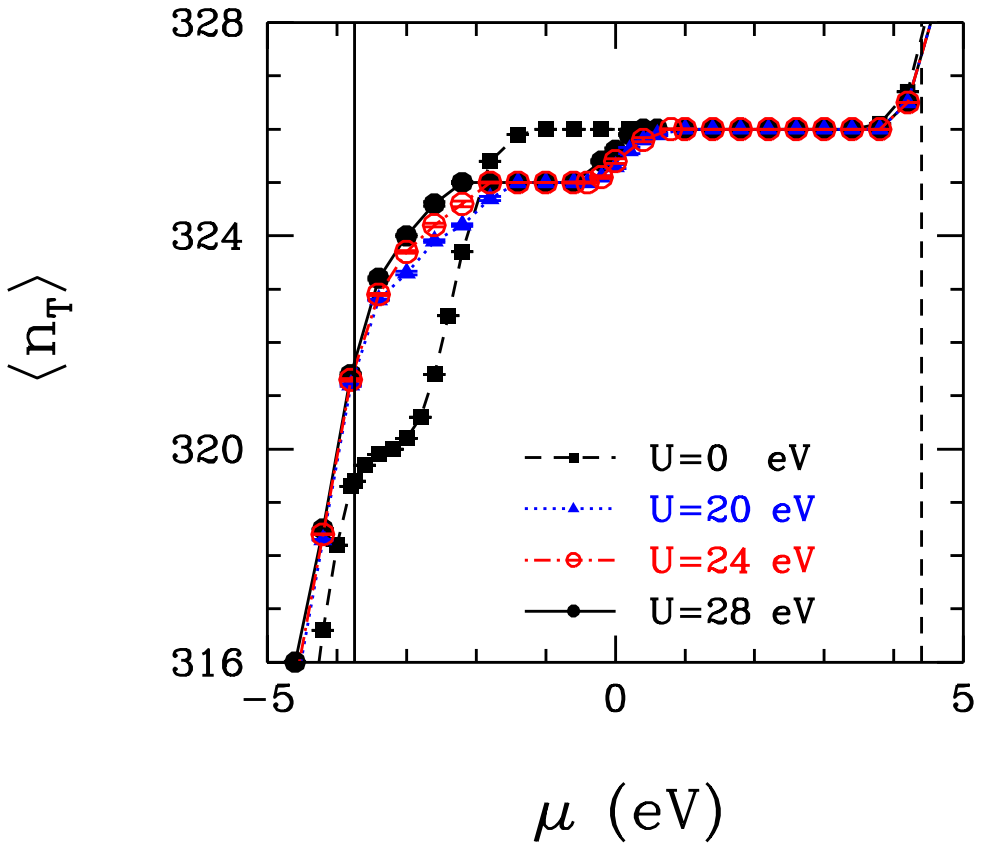

Figure 5.11. Total electron numbers of the N719 dye $\langle n_t \rangle = \langle n_d \rangle + \langle n_h \rangle$ as a function of the chemical potential μ. Here, results are shown for different values of the onsite Coulomb repulsion U. In addition, the vertical solid and dashed lines denote the HOMO and LUMO levels, respectively.

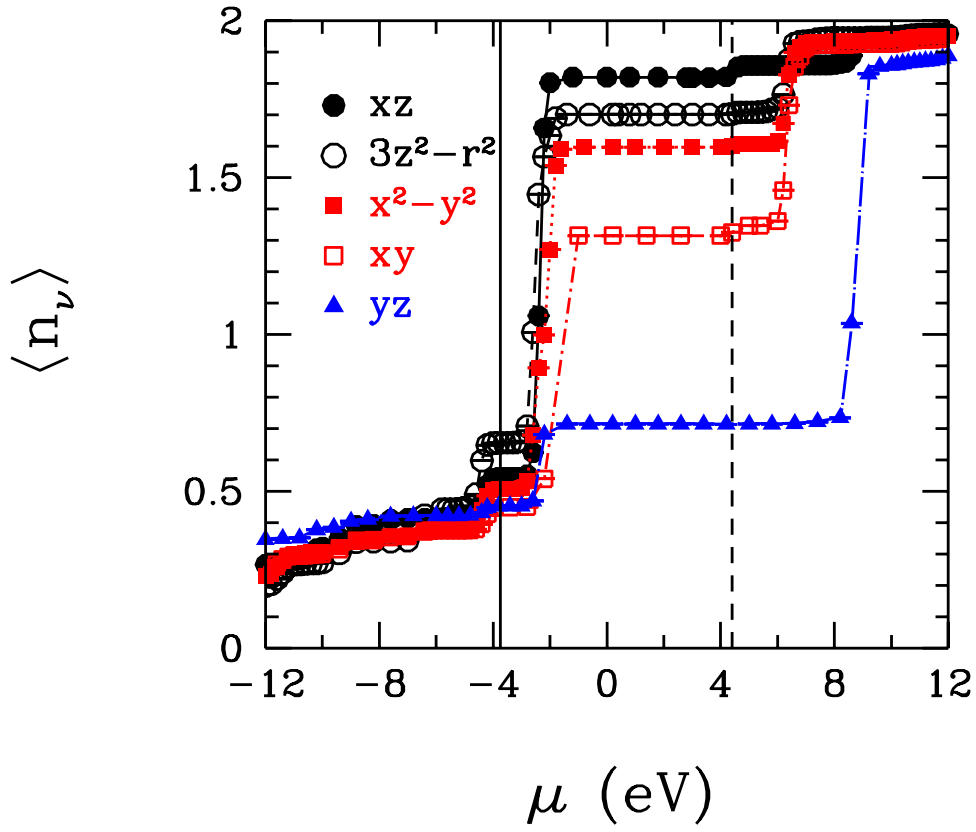

Figure 5.12. Occupation number of the $(4d_\nu)$ orbitals of ruthenium atom $\langle\, n_\nu \,\rangle$ plotted as a function of the chemical potential μ. Here, results are shown for the onsite coulomb repulsion $U = 0eV$. In addition, the vertical solid and dashed lines denotes the HOMO and LUMO levels, respectively.

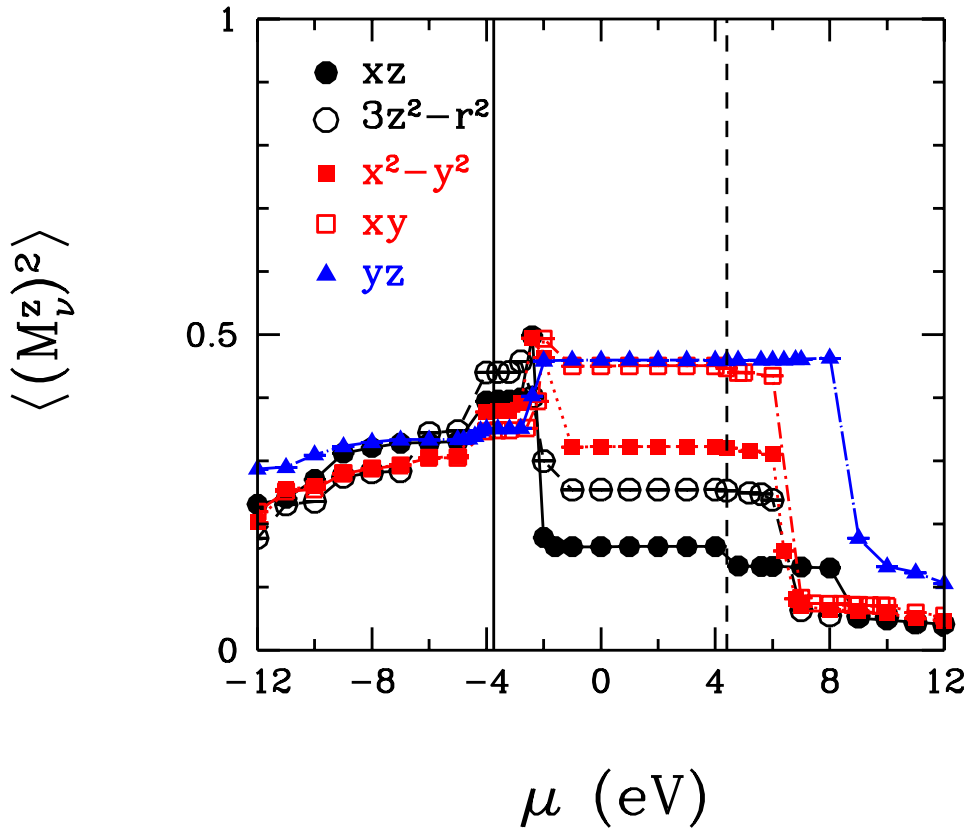

Figure 5.13. Square of the local magnetic moment of the $(4d_\nu)$ orbitals of ruthenium atom $\langle\,(M_\nu{}^z)^2\,\rangle$ plotted as a function of the chemical potential μ. Here, results are shown for the onsite coulomb repulsion $U = 0eV$. In addition, the vertical solid and dashed lines denote the HOMO and LUMO levels, respectively.

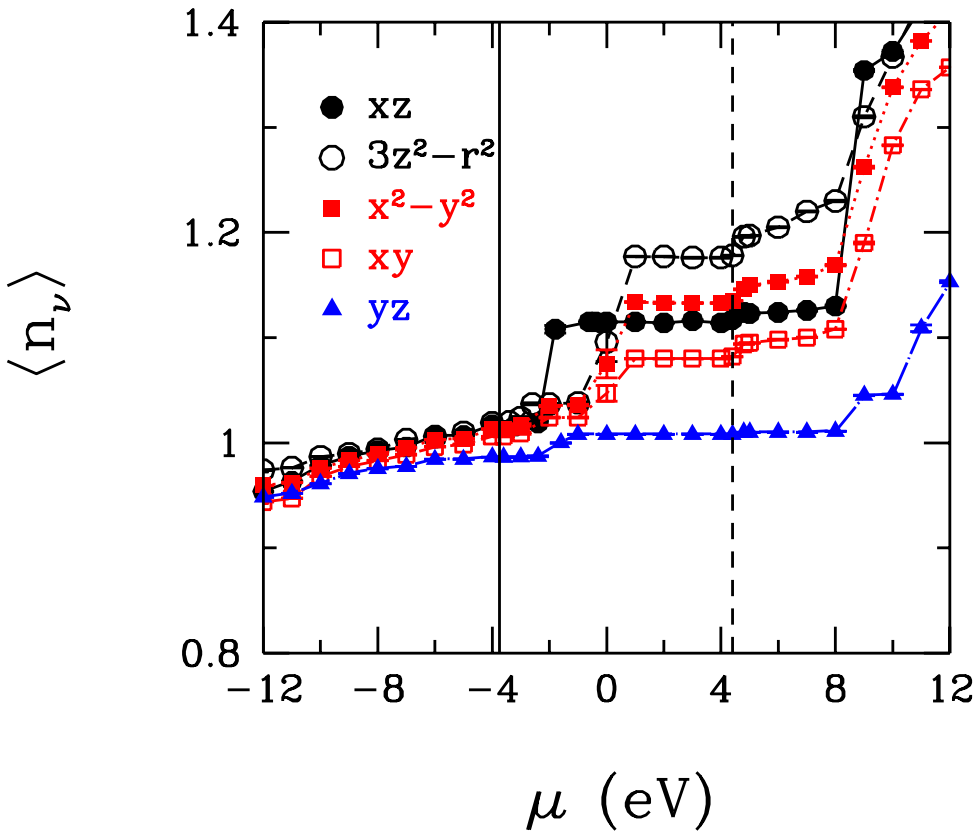

Figure 5.14. Occupation number of the $(4d_\nu)$ orbitals of ruthenium atom $\langle\, n_\nu \,\rangle$ plotted as a function of the chemical potential μ. Here, results are shown for the onsite coulomb repulsion $U = 20eV$. In addition, the vertical solid and dashed lines denote the HOMO and LUMO levels, respectively.

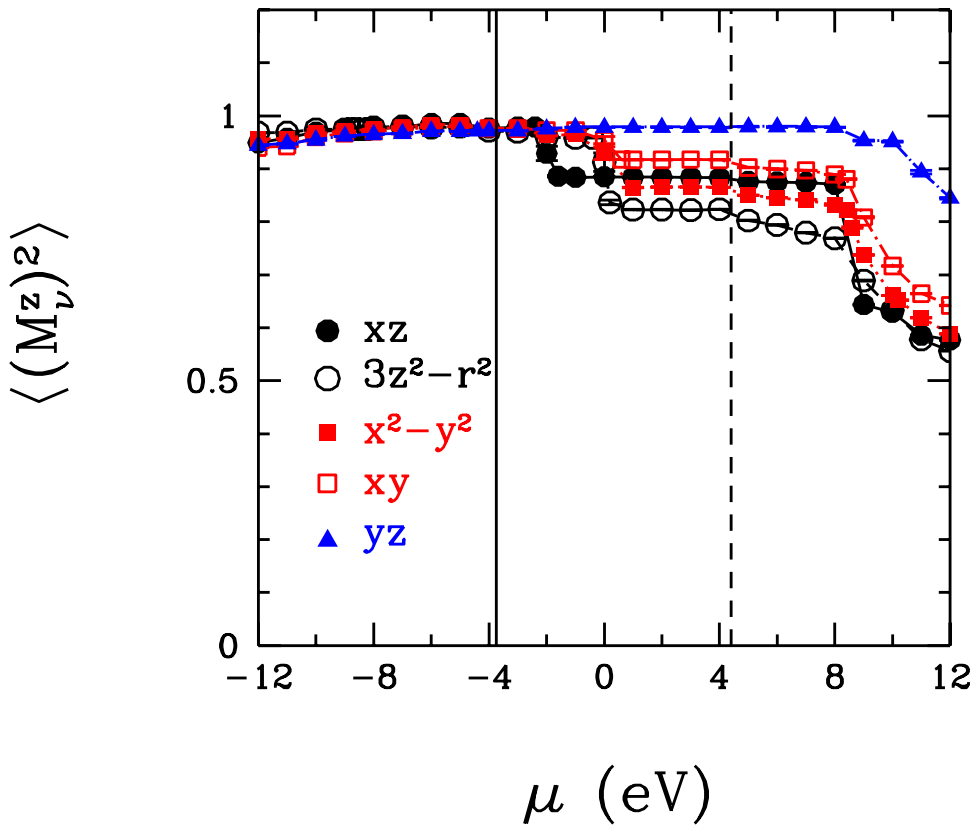

Figure 5.15. Square of the local magnetic moment of the $(4d_\nu)$ orbitals of ruthenium atom $\langle\,(M_\nu{}^z)^2\,\rangle$ plotted as a function of the chemical potential μ. Here, results are shown for the onsite coulomb repulsion $U = 20eV$. In addition, the vertical solid and dashed lines denote the HOMO and LUMO levels, respectively.

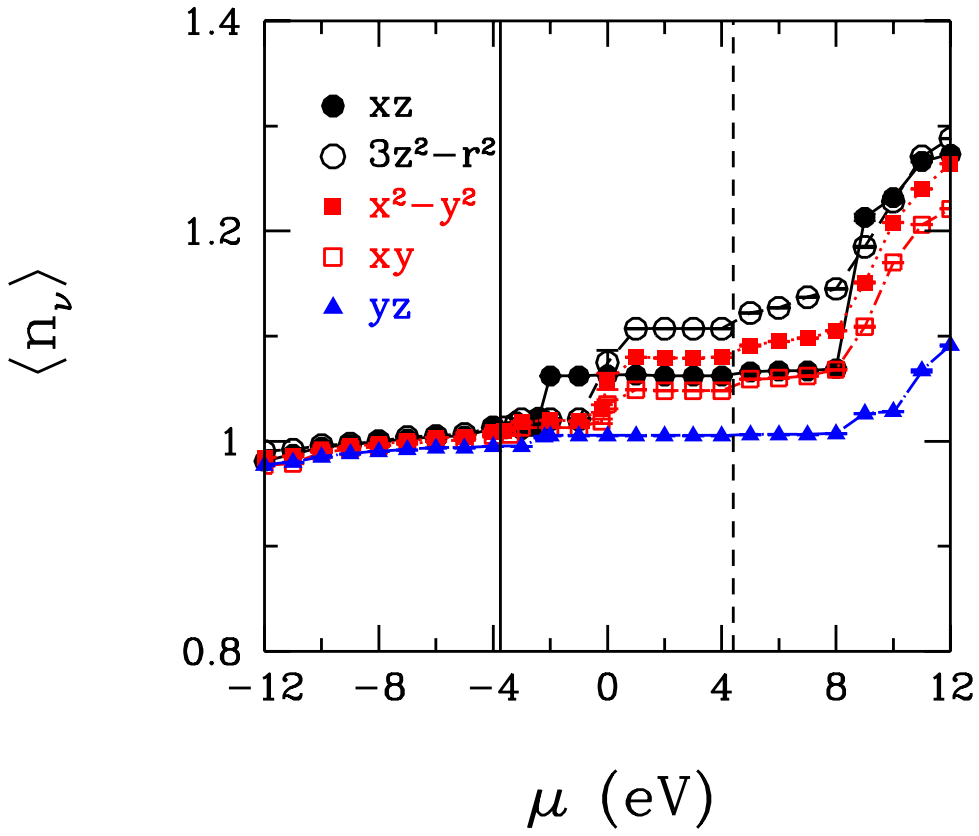

Figure 5.16. Occupation number of the $(4d_\nu)$ orbitals of ruthenium atom $\langle\, n_\nu \,\rangle$ plotted as a function of the chemical potential μ. Here, results are shown for the onsite coulomb repulsion $U = 24eV$. In addition, the vertical solid and dashed lines denote the HOMO and LUMO levels, respectively.

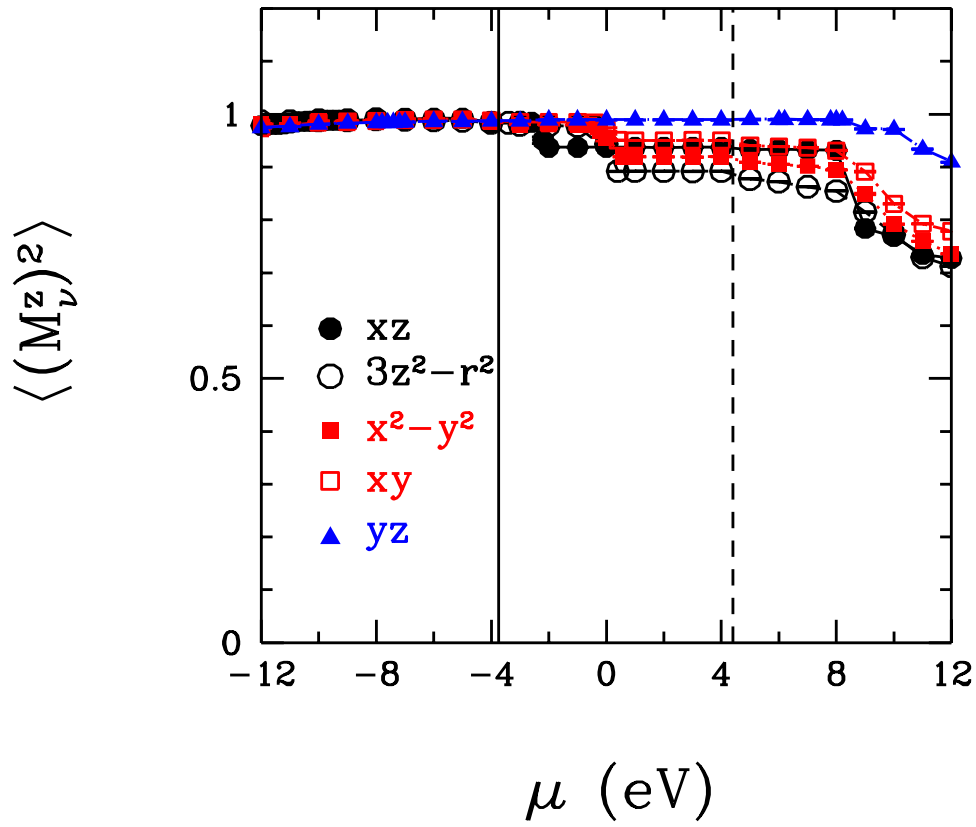

Figure 5.17. Square of the local magnetic moment of the $(4d_\nu)$ orbitals of ruthenium atom $\langle\,(M_\nu{}^z)^2\,\rangle$ plotted as a function of the chemical potential μ. Here, results are shown for the onsite coulomb repulsion $U = 24eV$. In addition, the vertical solid and dashed lines denote the HOMO and LUMO levels, respectively.

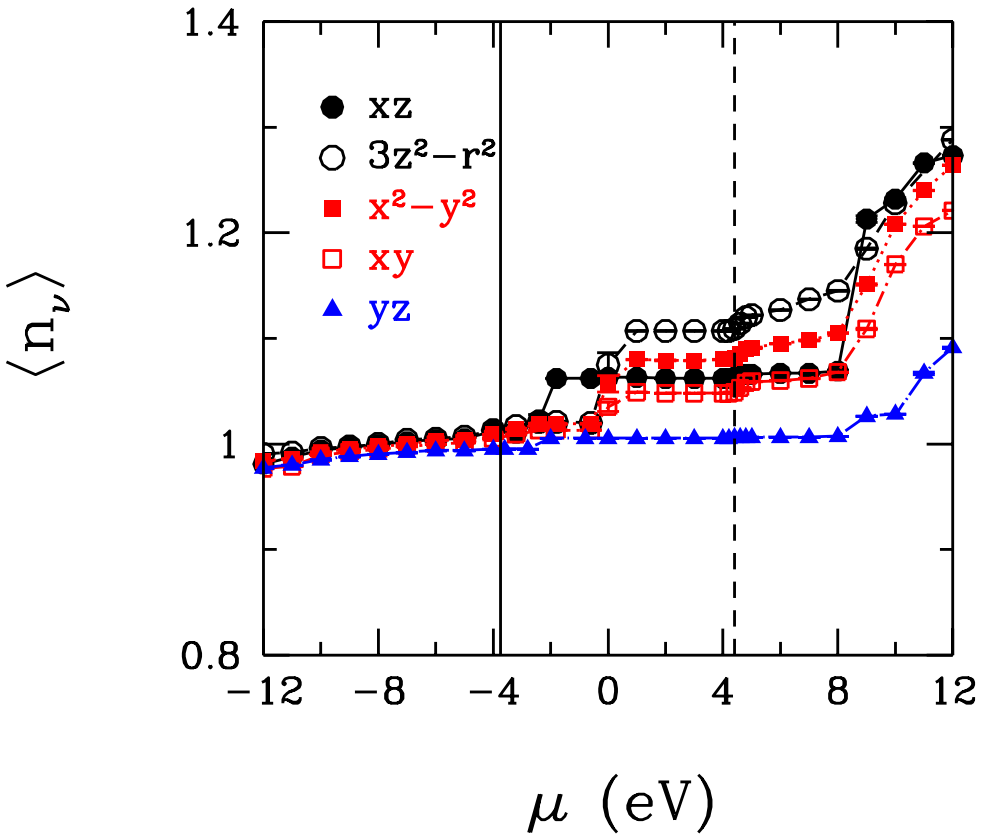

Figure 5.18. Occupation number of the $(4d_\nu)$ orbitals of ruthenium atom $\langle\, n_\nu \,\rangle$ plotted as a function of the chemical potential μ. Here, results are shown for the onsite coulomb repulsion $U = 28eV$. In addition, the vertical solid and dashed lines denote the HOMO and LUMO levels, respectively.

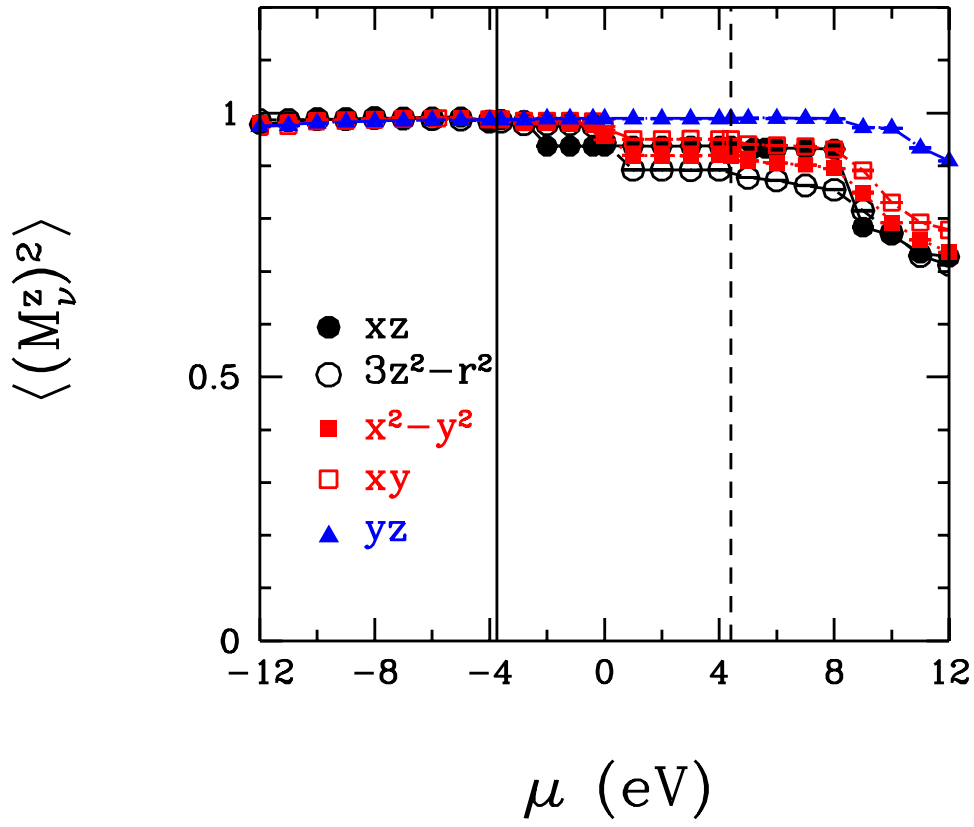

Figure 5.19. Square of the local magnetic moment of the $(4d_\nu)$ orbitals of ruthenium atom $\langle\,(M_\nu{}^z)^2\,\rangle$ plotted as a function of the chemical potential μ. Here, results are shown for the onsite coulomb repulsion $U = 28eV$. In addition, the vertical solid and dashed lines denote the HOMO and LUMO levels, respectively.

Occupation number of $4d_\nu$ orbitals of the ruthenium atom is decreased to nearly 5 after we did HF+QMC calculation. Total occupation number of the $4d_\nu$ orbitals of the ruthenium atom is 6.9 for $U = 0eV$, 5.5 for $U = 20eV$, 5.2 for $U = 24eV$, 5.1 for $U = 28eV$. Also we found occupation number of the host states of N719 dye is increased after QMC calculations. We see that total electron number of the sytem is became constant around 325 electron and when we reached chemical potential value $0eV$, total electron number of the sytem increase again Finally after $1eV$ for chemical potential value, total electron number of the sytem will be constant again and total electron number of the system is 326.

5.3.2. Density Function Theory + QMC Results

We use Anderson Hamiltonian parameter from Density Functional Theory for QMC calculations in this section. We found occupation number of host states of the N719 dye and occupation number of ($4d_\nu$) orbitals of the ruthenium atom for temperature 700K. In these calculations $\beta = \Delta\tau L$ are parameters of Hirsch-Fye algortihm and these values are $\Delta\tau = 0.3625$ and $L = 46$. Also we found square of local magnetic moment of ($4d_\nu$) orbitals of ruthenium atom for $T = 700K$. For magnetic moment calculations Hirsch-Fye parameters values are $\Delta\tau = 0.3625$ and $L = 46$. For impurity orbital calculations number of warm up sweeps are 1000 and number of measurement sweeps are 1000 and total electron number of the sytem calculations number of warm up sweeps and measurement sweeps are 100.

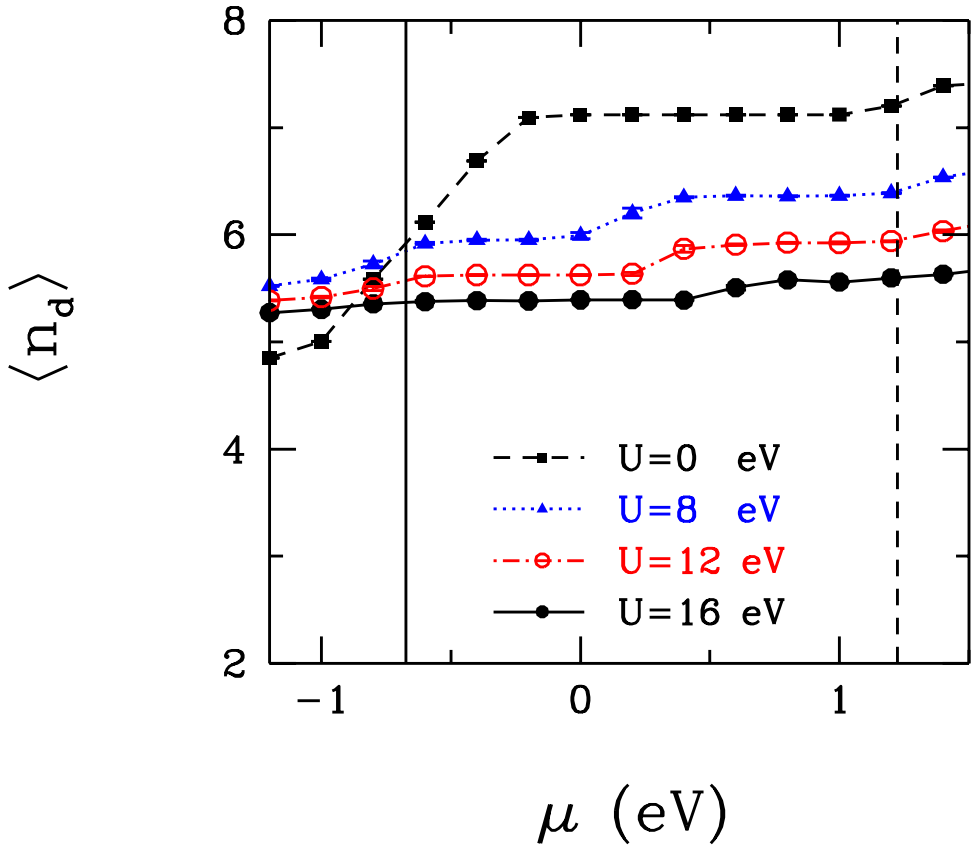

Figure 5.20. Occupation number of the $(4d_\nu)$ orbitals of the ruthenium atom $\langle\, n_d \,\rangle$ as a function of the chemical potential μ. Here, results are shown for different values of the onsite Coulomb repulsion U. In addition, the vertical solid and dashed lines denote the HOMO and LUMO levels, respectively.

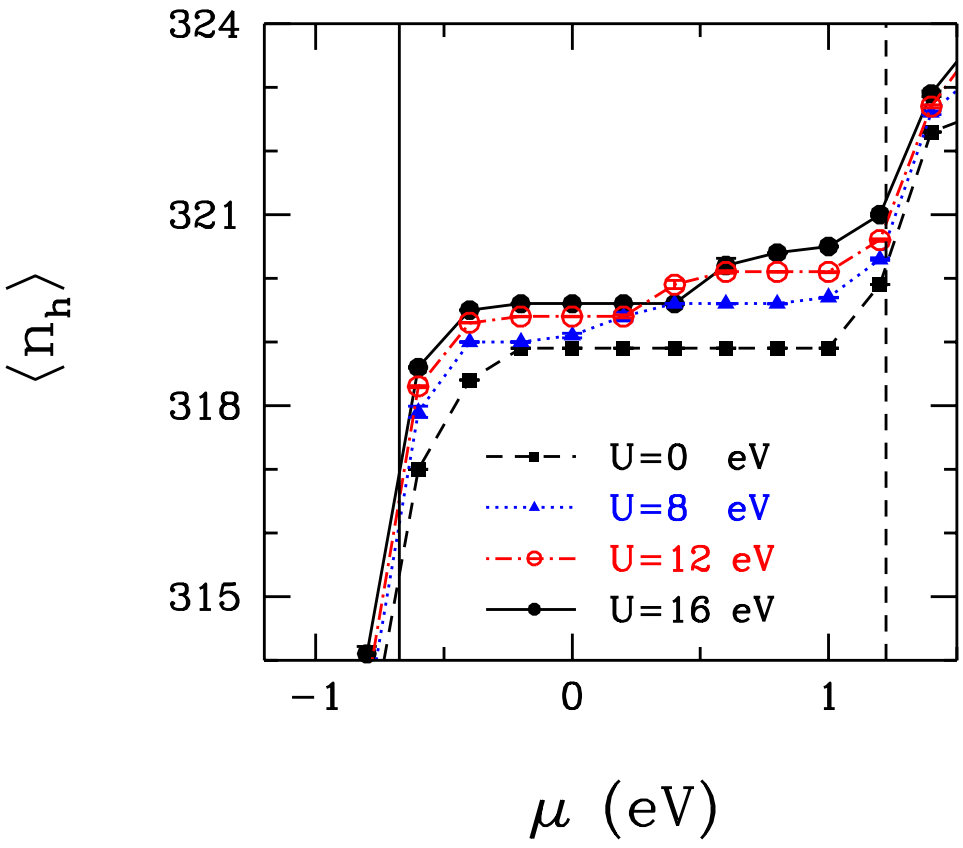

Figure 5.21. Occupation number of the host states of N719 dye $\langle n_h \rangle$ as a function of the chemical potential μ. Here, results are shown for different values of the onsite Coulomb repulsion U. In addition, the vertical solid and dashed lines denote the HOMO and LUMO levels, respectively.

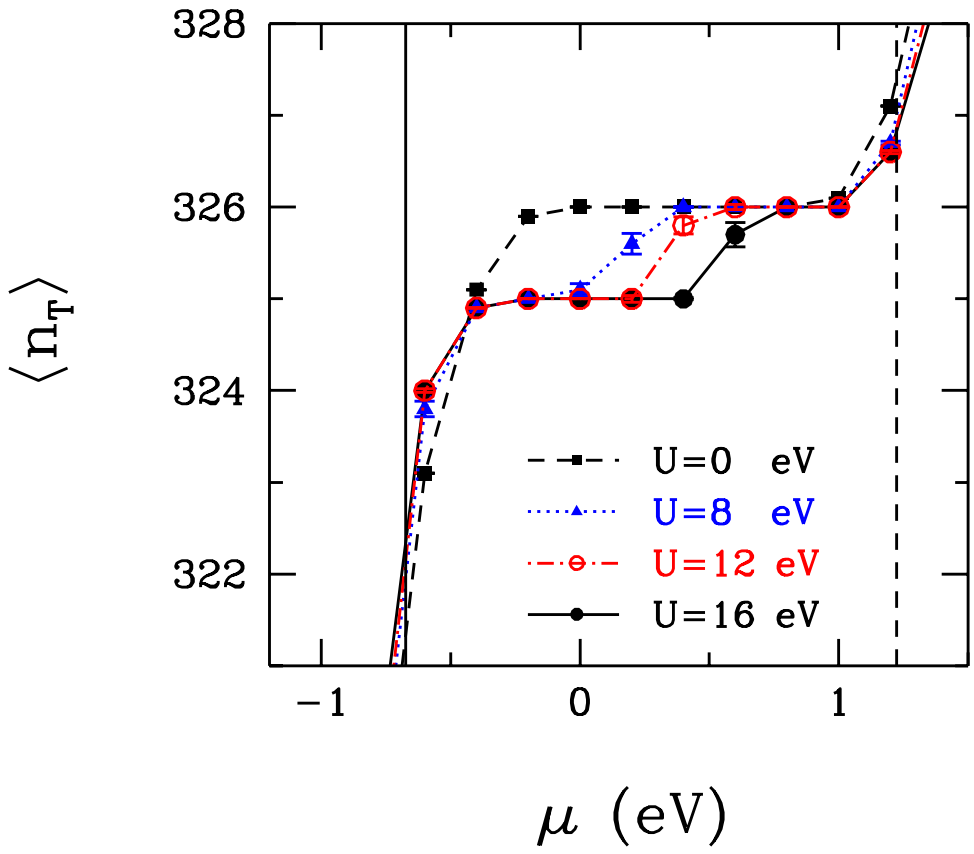

Figure 5.22. Total electron numbers of the N719 dye $\langle n_t \rangle = \langle n_d \rangle + \langle n_h \rangle$ as a function of the chemical potential μ. Here, results are shown for different values of the onsite Coulomb repulsion U. In addition, the vertical solid and dashed lines denote the HOMO and LUMO levels, respectively.

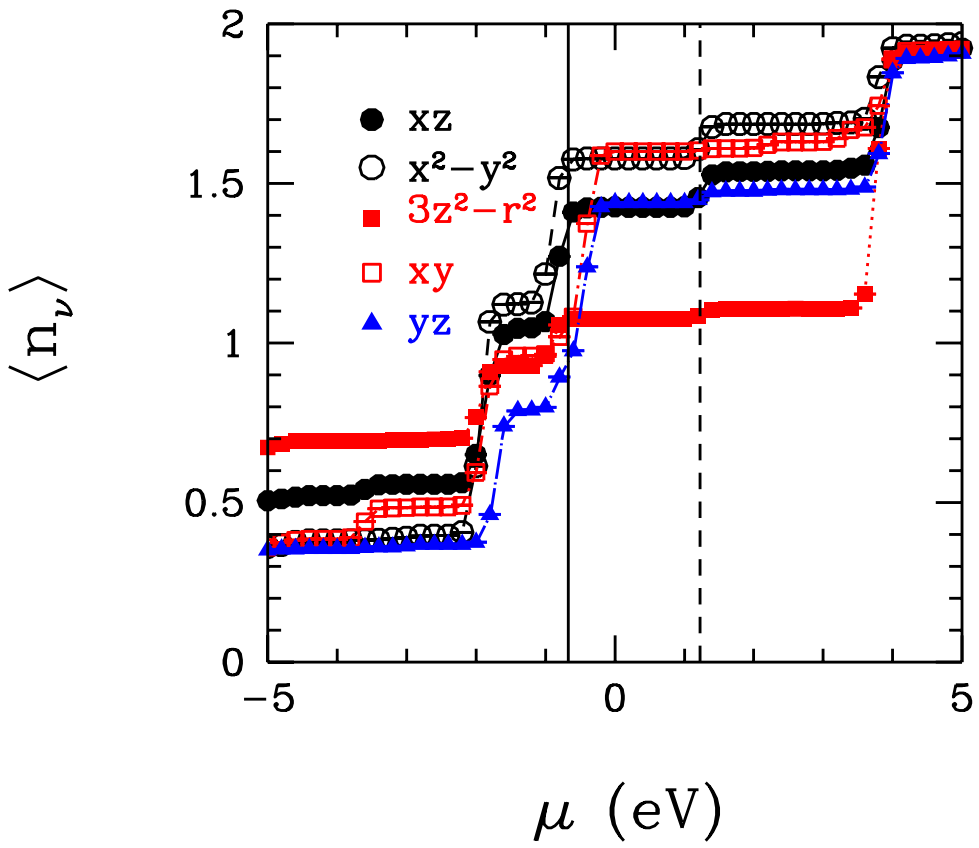

Figure 5.23. Occupation number of the $(4d_\nu)$ orbitals of ruthenium atom $\langle\, n_\nu \,\rangle$ plotted as a function of the chemical potential μ. Here, results are shown for the onsite coulomb repulsion $U = 0eV$. In addition, the vertical solid and dashed lines denotes the HOMO and LUMO levels, respectively.

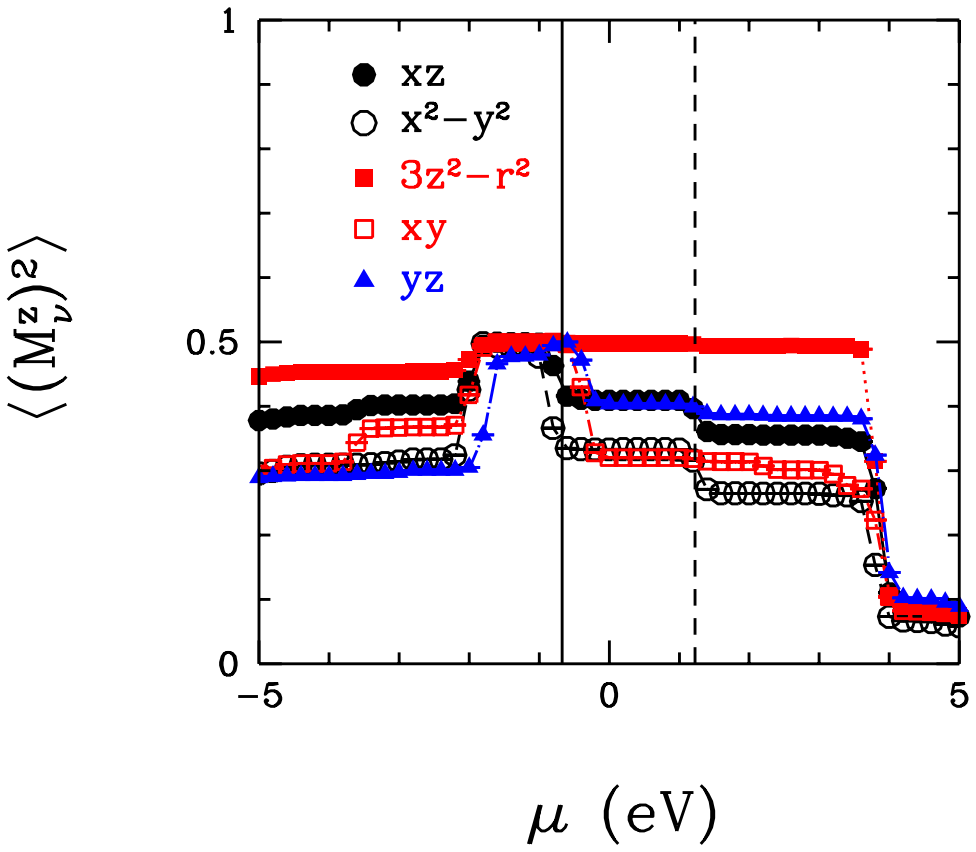

Figure 5.24. Square of the local magnetic moment of the $(4d_\nu)$ orbitals of ruthenium atom $\langle\,(M_\nu{}^z)^2\,\rangle$ plotted as a function of the chemical potential μ. Here, results are shown for the onsite coulomb repulsion $U = 0eV$. In addition, the vertical solid and dashed lines denote the HOMO and LUMO levels, respectively.

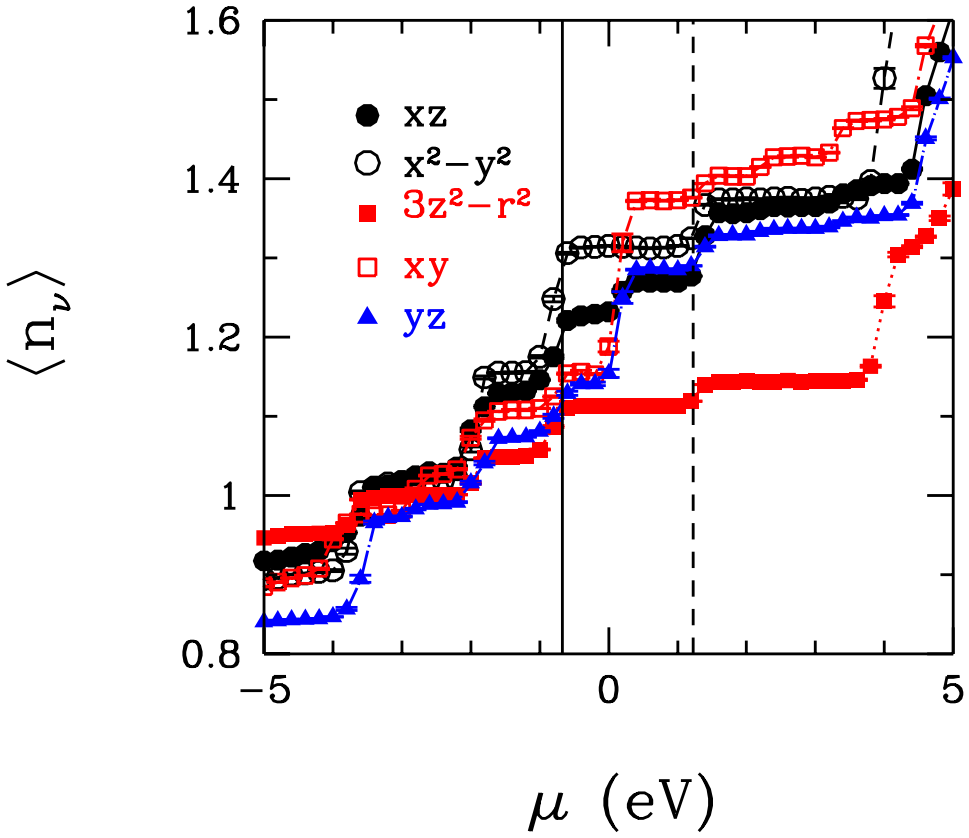

Figure 5.25. Occupation number of the $(4d_\nu)$ orbitals of ruthenium atom $\langle\, n_\nu \,\rangle$ plotted as a function of the chemical potential μ. Here, results are shown for the onsite coulomb repulsion $U = 8eV$. In addition, the vertical solid and dashed lines denotes the HOMO and LUMO levels, respectively.

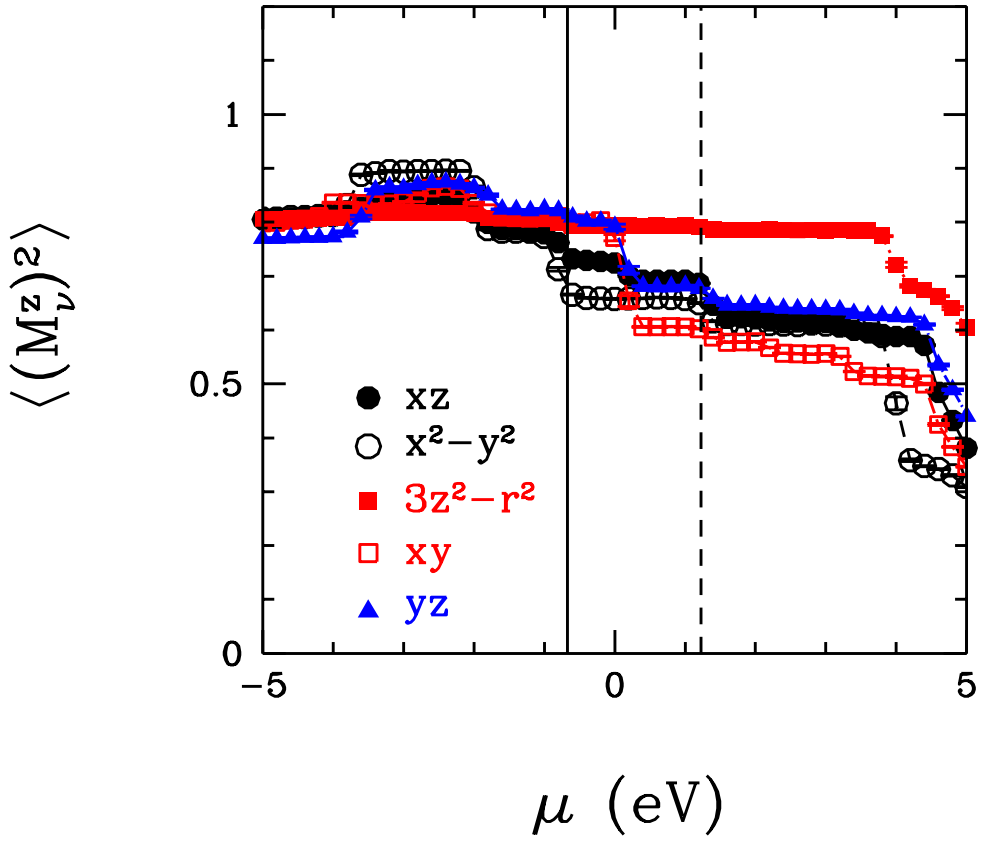

Figure 5.26. Square of the local magnetic moment of the $(4d_\nu)$ orbitals of ruthenium atom $\langle\,(M_\nu{}^z)^2\,\rangle$ plotted as a function of the chemical potential μ. Here, results are shown for the onsite coulomb repulsion $U = 8eV$. In addition, the vertical solid and dashed lines denote the HOMO and LUMO levels, respectively.

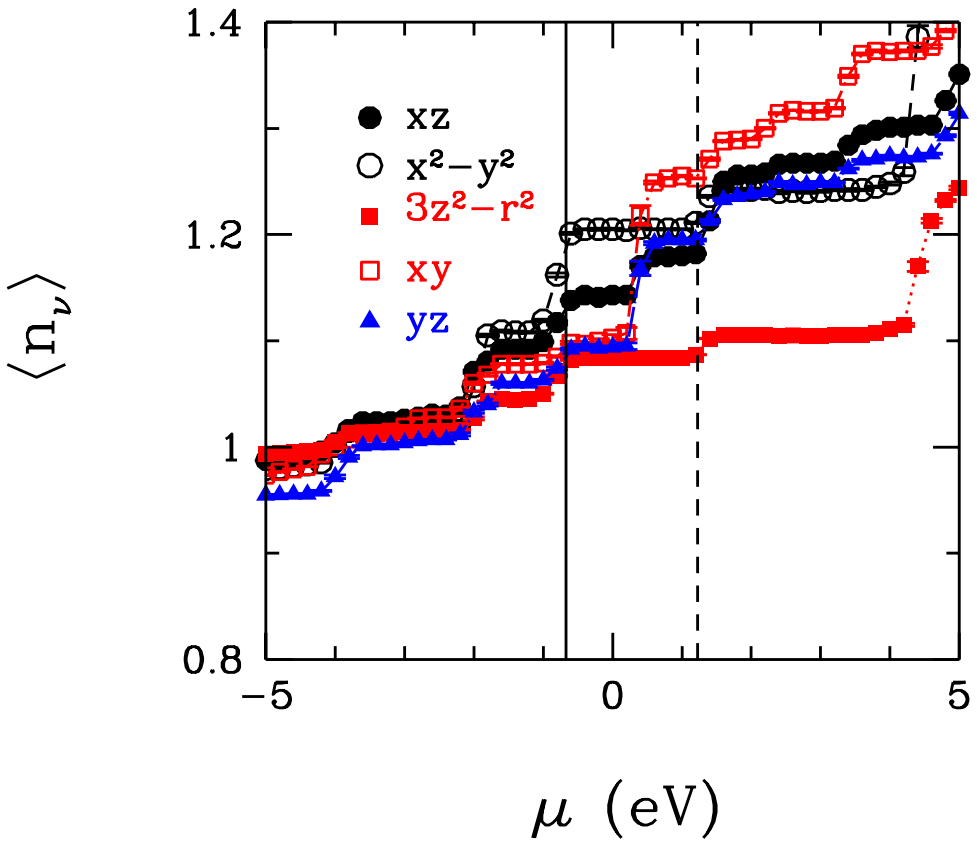

Figure 5.27. Occupation number of the $(4d_\nu)$ orbitals of ruthenium atom $\langle\, n_\nu \,\rangle$ plotted as a function of the chemical potential μ. Here, results are shown for the onsite coulomb repulsion $U = 12eV$. In addition, the vertical solid and dashed lines denotes the HOMO and LUMO levels, respectively.

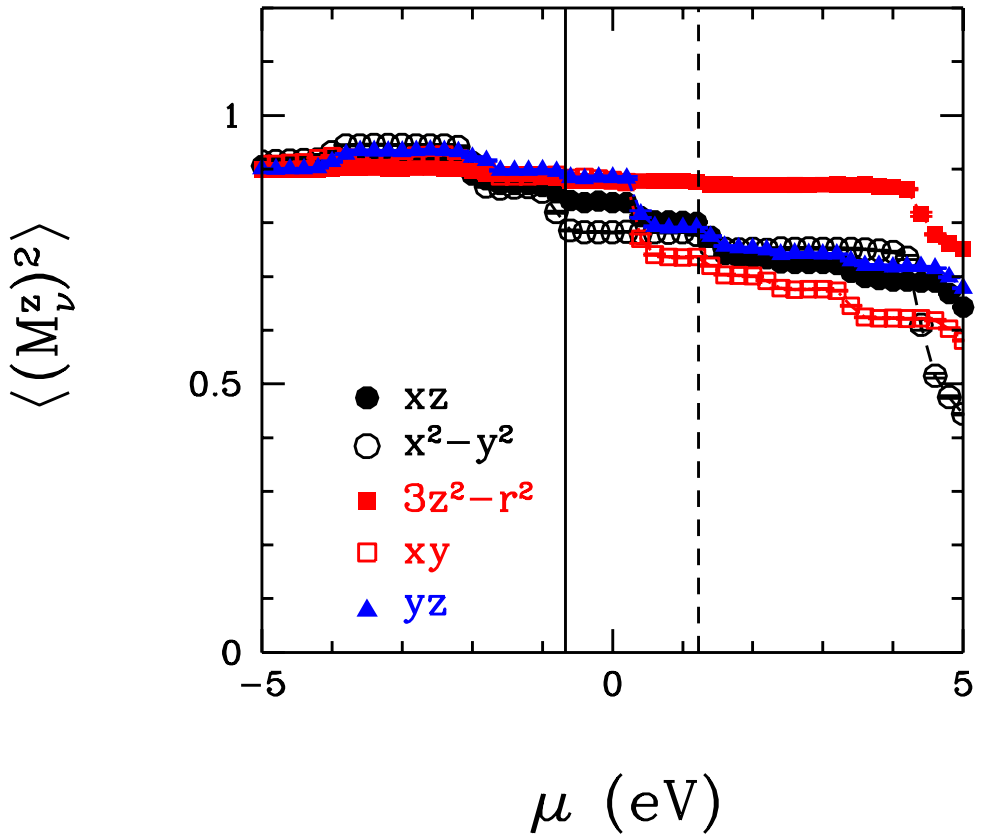

Figure 5.28. Square of the local magnetic moment of the $(4d_\nu)$ orbitals of ruthenium atom $\langle\,(M_\nu{}^z)^2\,\rangle$ plotted as a function of the chemical potential μ. Here, results are shown for the onsite coulomb repulsion $U = 12eV$. In addition, the vertical solid and dashed lines denote the HOMO and LUMO levels, respectively.

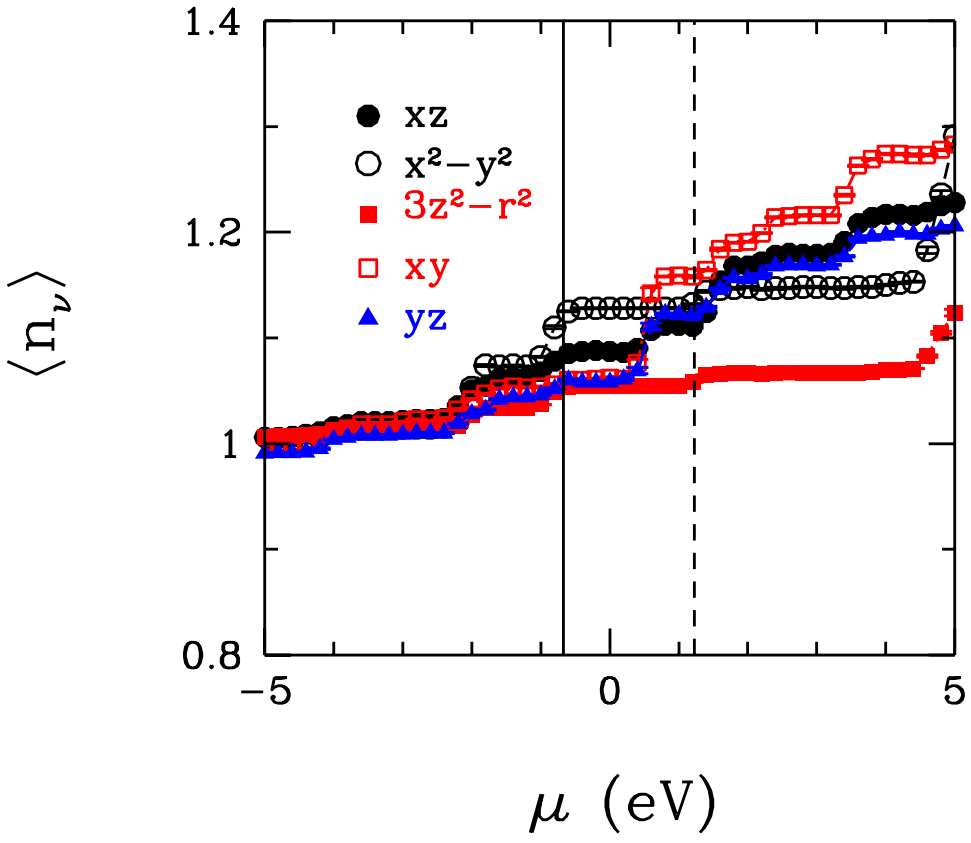

Figure 5.29. Occupation number of the $(4d_\nu)$ orbitals of ruthenium atom $\langle\, n_\nu \,\rangle$ plotted as a function of the chemical potential μ. Here, results are shown for the onsite coulomb repulsion $U = 16eV$. In addition, the vertical solid and dashed lines denotes the HOMO and LUMO levels, respectively.

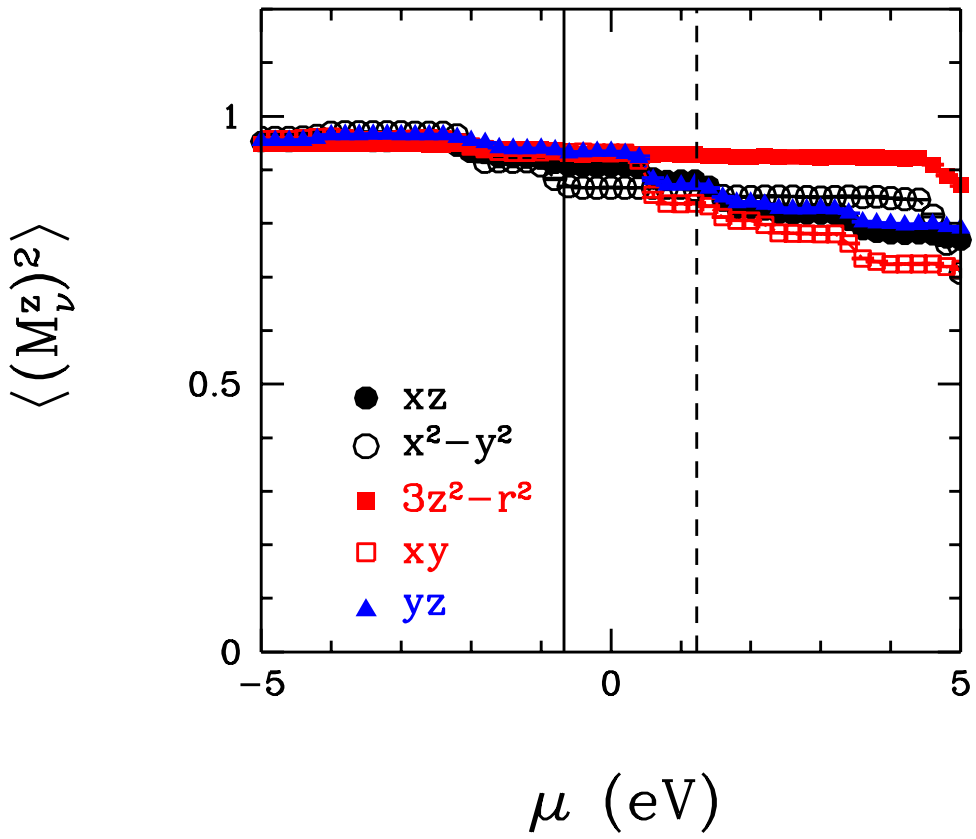

Figure 5.30. Square of the local magnetic moment of the $(4d_\nu)$ orbitals of ruthenium atom $\langle\,(M_\nu{}^z)^2\,\rangle$ plotted as a function of the chemical potential μ. Here, results are shown for the onsite coulomb repulsion $U = 16eV$. In addition, the vertical solid and dashed lines denote the HOMO and LUMO levels, respectively.

Occupation number of $4d_\nu$ orbitals of the ruthenium atom is decreased to nearly 5.5 after we did DFT+QMC calculation. Total occupation number of $4d_\nu$ orbitals of the ruthenium atom is 7.1 for $U = 0eV$, 6.3 for $U = 8eV$, 6 for $U = 12eV$, 5.5 for $U = 16eV$. Also we found occupation number of the host states of N719 dye is increased after QMC calculations. We see that total electron number of the sytem is became constant around 325 electron and when we reached chemical potential value $0eV$, total electron number of the sytem increase again Finally after $0.5eV$ for chemical potential value, total electron number of the sytem will be constant again and total electron number of the system is 326 .

5.3.3. Comparation between DFT + QMC and Hartree-Fock +QMC

There is very important main differences of pure DFT and HF calculation. In DFT, we are taking acount electron-electron correlation effects and this gives different energy band structure for HF and DFT calculations. In DFT calculations, band gap of the system is narrower when we compare it with HF calculations. We use B3LYP functional with local density approximation for DFT and this is the reason why band gap is narrower, when we compare it with HF calculations.

When we did DFT+QMC and HF+QMC calculation, we see that HOMO and LUMO level of the N719 dye changed. For DFT+QMC calculation new HOMO and LUMO levels are $0.4eV$ and $1eV$ for $U = 8eV$, $0.5eV$ and $1eV$ for $U = 12eV$, $0.8eV$ and $1eV$ for $U = 16eV$. For HF+QMC calculation new HOMO and LUMO levels are $1.1eV$ and $3.8eV$ for $U = 20eV$, $1eV$ and $3.8eV$ for $U = 24eV$, $0.8eV$ and $3.8eV$ for $U = 28eV$.

We found there are new states between HOMO and LUMO levels for both DFT+ QMC and HF+QMC calculations. These new states gives different magnetic properties to the system which we cant see from just pure DFT or HF calculations. If we look occupation number of $4d_\nu$ orbitals of ruthenium atom, we can see these new states. Occupation number of the yz, xz, xy orbitals of the ruthenium atom are increasing in HOMO and LUMO levels for all values of U for DFT+QMC calculation and occupation number of $3z^2 - r^2$ and $x^2 - y^2$ orbitals of the ruthenium atom are constant in HOMO and LUMO levels for DFT+QMC calculations. Occupation number of the $xy, x^2 - y^2, 3z^2 - r^2$ orbitals of the ruthenium atom are increasing in HOMO and LUMO levels for all values of U and occupation number of yz and xz orbitals of the ruthenium atom are constant in HOMO and LUMO level for HF+QMC calculations.

CHAPTER 6

CONCLUSION

The magnetic and electronic properties of N719 dye has been shown by using Hirsch-Fye QMC algorithm with the impurity Anderson model. $4d$ orbitals of the ruthenium atom defined as impurity part and the other orbitals of the N719 dye defined as host part. Anderson model parameters are calculated from Hartree-Fock Theory and Density Functional Theory. We take into account onsite Coulomb interaction by using HF+QMC and DFT+QMC method. Then, we compared HF and DFT calculations and HF+QMC and DFT+QMC calculations.

If we look $U = 0eV$ QMC results, we can say that these results can give an ophinion for pure HF and DFT results. Occupation number of the $4d_\nu$ orbitals of the ruthenium atom is constant for DFT+QMC and HF+QMC calculation in HOMO and LUMO levels and occupation number of $4d_\nu$ orbitals are changing in HOMO and LUMO levels for DFT+QMC and HF+QMC calculation for increased value of onsite Coulomb interaction value U. Also we found there are new states in HOMO and LUMO levels for both DFT+QMC and HF+QMC calculations. Occupation number of the $4d_\nu$ orbitals of ruthenium atom are nearly doubly occupied for $U = 0eV$ in DFT+QMC and HF+QMC calculation. When we increased onsite Coulomb interaction value, we found that occupation numbers of the $4d_\nu$ orbitals of the ruthenium atom is decreasing nearly 1 and we found that these orbitals became magnetic when we increase onsite Coulomb interaction values for DFT+QMC and HF+QMC calculations.

We looked energy gap value from litarature for N719 dye experimently and it is $2.25eV$ [40]. We found energy gap value from DFT $1.90eV$ and from Hartree-Fock $8.15eV$. We found that in our QMC calculations HOMO and LUMO level of the N719 dye has changed. In DFT+QMC calculation new energy gap values are $0.6eV$ for $U = 8eV$, $0.4eV$ for $U = 12eV$ and $0.2eV$ for $U = 16eV$. In HF+QMC calculation new energy gap values are $2.7eV$ for $U = 20eV$, $2.8eV$ for $U = 24eV$, $3.0eV$ for $U = 28eV$. Therefore we can say that most similar results can be found from HF+QMC for band gap values for N719 dye.

Pure DFT is very good method for describing electronic and magnetic properties of system. It is very quick and can give good results for fining band sturcture of the system. But from pure DFT we can not find correct magnetic properties of the system. If

we do HF+QMC method we can find correct band structure also magnetic properties of the system. Also DFT+QMC method and HF+QMC method are very similar for finding magnetic properties of the system but HF+QMC method is better than DFT+QMC method for finding band structure of the system. HF method is like more primitive version of DFT method but for advanced method like DFT+QMC or HF+QMC, HF method is better then DFT to construnct more advance models.

In the future, if we look other ruthenium-based dyes with Hirsch-Fye Quantum Monte Carlo algorithm, we can find different magnetic properties. Molecular sturcture of different ruthenium-based dyes causes different magnetic properties and these differences in the magnetic properties of dye molecules gives different efficiency and different stabilities in DSSC. If we understand, what magnetic properties will raise when we changed molecular structure of the dye molecules, we can find more efficient and more stable dye molecules.

REFERENCES

[1] Brian O'Regan and Micheal Grätzel. A low cost, high efficiency solar cell based on dye-sensitized collodial ti02 films. *Nature (London, United Kingdom)*, 1991.

[2] Brian O'Regan. The "invention" of the dssc.

[3] Seigo Ito. Investigation of dyes for dye-sensitized solar cells: Ruthenium-complex dyes, metal-free dyes, metal-complex porphyrin dyes and natural dyes.

[4] Michio Matsumura, Shigeyuki Matsudaira, Hiroshi Tsubomura, and Masasuke Takata andHiroaki Yanagida. Dye sensitization and surface structures of semiconductor electrodes. *Industrial & Engineering Chemistry Research*, 1980.

[5] W.-Y. Wong, editor. *Organometallics and Related Molecules for Energy Conversion, Green Chemistry and Sustainable Technology*. Springer, 2015.

[6] Kieron Burke, Lucas Wagner, Miles Stoudenmire, and Steve White. Failures of density functional theory for strongly correlated systems using density-matrix renormalization group, 2013.

[7] P.W. Anderson. Localized magnetic states in metals. *Physical Review*, 1961.

[8] M. J. Frisch, G. W. Trucks, H. B. Schlegel, G. E. Scuseria, M. A. Robb, J. R. Cheeseman, G. Scalmani, V. Barone, B. Mennucci, G. A. Petersson, H. Nakatsuji, M. Caricato, X. Li, H. P. Hratchian, A. F. Izmaylov, J. Bloino, G. Zheng, J. L. Sonnenberg, M. Hada, M. Ehara, K. Toyota, R. Fukuda, J. Hasegawa, M. Ishida, T. Nakajima, Y. Honda, O. Kitao, H. Nakai, T. Vreven, J. A. Montgomery, Jr., J. E. Peralta, F. Ogliaro, M. Bearpark, J. J. Heyd, E. Brothers, K. N. Kudin, V. N. Staroverov, R. Kobayashi, J. Normand, K. Raghavachari, A. Rendell, J. C. Burant, S. S. Iyengar, J. Tomasi, M. Cossi, N. Rega, J. M. Millam, M. Klene, J. E. Knox, J. B. Cross, V. Bakken, C. Adamo, J. Jaramillo, R. Gomperts, R. E. Stratmann, O. Yazyev, A. J. Austin, R. Cammi, C. Pomelli, J. W. Ochterski, R. L. Martin, K. Morokuma, V. G. Zakrzewski, G. A. Voth, P. Salvador, J. J. Dannenberg, S. Dapprich, A. D. Daniels, Ã. Farkas, J. B. Foresman, J. V. Ortiz, J. Cioslowski, and D. J. Fox. Gaussian 09

Revision A.1. Gaussian Inc. Wallingford CT 2009.

[9] E. D. Glendening, A. E. Reed J. E. Carpenter J. A. Bohmann C. M. Morales C. R. Landis J, K. Badenhoop, and University of Wisconsin Madison (2013). F. Weinhold, Theoretical Chemistry Institute. Nbo version 6.0.

[10] M. K. Nazeeruddin, A. Kay, I. Podicio, R. Humphy-Baker, E. Müller, P. Liska, N. Vlachopoulos, and M. Grätzel. Conversion of light to electricity by cis-xzbis(2,2â-bipyridyl-4,4â-dicarboxylate)ruthenium(11) charge-transfer sensitizers (x = c1-, br-, i-, cn-, and scn-) on nanocrystalline ti02 electrodes. *Journal American Chemical Society*, 1993.

[11] M. K. Nazeeruddin, F. D. Angelis, S. Fantacci, A. Selloni, G. Viscardi, P. Liska, S. Ito, B. Takeru, and M. Grätzel. Combined experimental and dft-tddft computational study of photoelectrochemical cell ruthenium sensitizers. *Journal of American Chemical Society*, 2005.

[12] Peng Wang, Shaik M. Zakeeruddin, Jacques E. Moser, Mohammad K. Nazeeruddin, Takashi Sekiguchi, and Michael Grätzel. A stable quasi-solid-state dye-sensitized solar cell with an amphiphilic ruthenium sensitizer and polymer gel electrolyte. *Nature Materials*, 2003.

[13] Hans Desilvestro and Yanek Hebting. Ruthenium-based dyes for dye solar cells.

[14] W. Heisenberg. Mehrkörperproblem und resonanz in der quantenmechanik. 1926.

[15] P. A. M. Dirac. on the theory of quantum mechanics. 1926.

[16] Frank Jensen. *Introduction to Computational Chemistry*. Wiley, 2007.

[17] C. David Sherill. An introduction to hartree-fock molecular orbital theory, 2000.

[18] Hande Toffoli. Lecture Notes: The Hartree Fock Method.

[19] Pekka Manninen. Lecture notes for the course advanced computational chemistry.

[20] T. Tsuneda. *Density Functional Theory in Quantum Chemistry*. Springer, 2014.

[21] Sergio Boixo. Applied quantum mechanics.

[22] P. Hohenberg and W. Kohn. Inhomogeneous electron gas. *Physical Review*, 1964.

[23] W. Kohn and L. J. Sham. Self-consistent equations including exchange and correlation effects. *Physical Review*, 1965.

[24] F. D. M. Haldane and P. W. Anderson. Simple model of multiple charge states of transition-metal impurities in semiconductors. *Physical Review B*, 1976.

[25] Selma Mayda. Electronic correlations in metalloproteins: A quantum monte carlo study. Master's thesis, Izmir Institute of Technology, 2013.

[26] Zafer Kandemir. Mapping of the electronic structure of metalloproteins onto multi orbital anderson model using the density functional theory. Master's thesis, Izmir Institute of Technology, 2013.

[27] M. Karolak, G. Ulm, T. O. Wehling, V. Mazurenko, A. Poteryaev, and A. I. Lichenstein. Double counting in lda plus dmft, the example of nio. *Journal of Electron Spectroscopy and Related Phenomena*, 2010.

[28] Roy Dennington, Todd Keith, and John Millam. Gaussview Version 5, 2009. Semichem Inc., Shawnee Mission KS.

[29] Florian Schiffmann, Joost VandeVondele, Jürg Hutter, Ronny Wirz, Atsushi Urakawa, and Alfons Baiker. Protonation-dependent binding of ruthenium bipyridyl complexes to the anatase(101) surface. *Physical Chemistry C*, 2010.

[30] Yali Sun. *The Developement of Novel Ru(II) Polyprdyl Complexes for Application in Dye Sensitized Solar Cells*. PhD thesis, 2009.

[31] A. D. Becke. Densityfunctional thermochemistry. iii. the role of exact exchange. *Journal of Chem. Phys.*, 1993.

[32] Chengteh Lee, Weitao Yang, and Robert G. Parr. Development of the colle-salvetti correlation-energy formula into a functional of the electron density. *Phys. Rev. B*, 1988.

[33] S. H. Vosko, L. Wilk, and M. Nusair. Accurate spin-dependent electron liquid correlation energies for local spin density calculations: a critical analysis. *Canadian Journal of Physics*, 1980.

[34] P. J. Stephens, F. J. Devlin, C. F. Chabalowski, and M. J. Frisch. Ab initio calculation of vibrational absorption and circular dichroism spectra using density functional force fields. *Journal of Phys. Chem.*, 1994.

[35] jr. T. H. Dunning and P. Jeffrey Hay. In modern theoretical chemistry. *Plenum*, 1977.

[36] P. Jeffrey Hay and W. R. Wadt. Ab initio effective core potentials for molecular calculations. potentials for k to au including the outermost core orbitals. *Journal of Chem. Phys.*, 1985.

[37] P. Jeffrey Hay and W. R. Wadt. Ab initio effective core potentials for molecular calculations. potentials for the transition metal atoms sc to hg. *The Journal of chemical physics*, 1985.

[38] W. R. Wadt and P. Jeffrey Hay. Ab initio effective core potentials for molecular calculations. potentials for main group elements na to bi. *Chem. Phys.*, 1985.

[39] J. E. Hirsch and R. M. Fye. Monte carlo method for magnetic impurities in metals. *Physical Review Letters*, 1986.

[40] Jin Zhang, Chunhui Yu, Lili Wang, Yizhi Li, Yuhang Ren, and Kai Shum. Energy barrier at the n719 dye/cssni 3 interface for photogenerated holes in dye sensitized solar cells. *Scientific Reports*, 2014.

[41] M. Born and R. Oppenheimer. Zur quantentheorie der molekeln. *Annalen der Physik*, 1927.

[42] M. Born and V. A. Fock. Beweis des adiabatensatzes. *Zeitschrift für Physik A*, 1928.

[43] Alan E. Reed, Larry A. Curtiss, and Frank Weinhold. Intermolecular interactions from a natural bond orbital, donor-acceptor viewpoint. *Chemical Reviews*, 1988.

[44] Viktor Oudovenko. Lecture note: Quantum monte carlo method in details.

APPENDIX A

THE BACKGROUND OF HARTREE-FOCK THEORY

A.1. Mandy Body Problem

The Adiabatic and Born-Openheimer approximation states that the total non-relativistic Hamiltonian H_{tot} can be written as kinetic and potential energies of the nuclei and electron [41, 42].

$$H_{tot} = T_n + T_e + V_{ne} + V_{ee} + V_{nn} \tag{A.1}$$

Here, T_n is kinetic energy of nuclei,

$$T_n = \sum_{a}^{N_{nuclei}} \frac{1}{2} {\nabla_a}^2 \tag{A.2}$$

T_e is kinetic energy of electrons,

$$T_e = \sum_{i}^{N_{el}} \frac{1}{2} {\nabla_i}^2 \tag{A.3}$$

V_{ne} is potential energy between nuclei and electrons,

$$V_{ne} = \sum_{a}^{N_{nuclei}} \sum_{i}^{N_{el}} \frac{Z_a}{|R_a - r_i|} \tag{A.4}$$

V_{ee} is potential energy between electron and electron,

$$V_{ee} = \sum_{i}^{N_{el}} \sum_{j>i}^{N_{el}} \frac{1}{|r_i - r_j|} \tag{A.5}$$

V_{nn} is potential energy between nuclei and nuclei.

$$V_{nn} = \sum_{a}^{N_{nuclei}} \sum_{b>a}^{N_{nuclei}} \frac{Z_a Z_b}{|R_a - R_b|} \tag{A.6}$$

Here, Z denotes charge of nuclei, R denotes position of nuclie and r, denotes position of electrons. Subindex a,b represent nuclei position and i,j electrons position. If the Hamiltonian is transformed to the center of mass system it can be written as

$$H_{tot} = T_n + H_e + H_{mp} \tag{A.7}$$

$$H_e = T_e + V_{ne} + V_{ee} + V_{nn} \tag{A.8}$$

$$H_{mp} = \frac{-1}{2M_{tot}} (\sum_{i}^{N_{el}} \nabla_i)^2 \tag{A.9}$$

Here, H_e is the Electronic Hamiltonian, H_{mp} is the Mass Polarization Hamiltonian and M_{tot} denote total mass of the nuclei, N_{el} denote total electron number of system [16, 18–21].

A.2. Hartree-Fock Approximation

Our main purpose is solving Electronic Hamiltonian and first thing to do that is construct Schrodinger Equation. For solving Schrodinger Equation we need to choose a trial wave function to describe our system. Spin dependence of wave function can be think as $|\alpha>$ and $|\beta>$ spin functions and they obey orthogonality relations,

$$< \alpha|\alpha >=< \beta|\beta >= 1 \tag{A.10}$$

$$< \alpha|\beta >=< \beta|\alpha >= 0 \tag{A.11}$$

For solving Electronic Schrodinger Equation our first assumption is Hartree-Fock approximation. This method states that true N-body ground state wave function can be approximated by a single slater determinant. So trial wave function's spatial part has to be contruct from slater determinants. If we take all possible single slater determinants into account, it will be the exact wave function of the system. But it is impossible to solve numerically in that case. Therefore trial wave function constructed from one slater determinants accourding to Hartree-Fock approximation. Another question is how we choose one the slater determinant from all slater determinants [14–16]. Answer is the system which we are dealing has to be in the ground state accourding to Hartree-Fock approximation so we choose one slater determinant from all other one which minimize the system's energy.

In Hartree-Fock approximation interaction between particles are approximated, either by neglecting all but the most important one or by taking all interactions into account in an avarage fashion. So in this approximation electrons interactions are taking as avarage fashion and neglecting correlation between electrons.

Now we are ready to construct wave function as slater determinat for N electron and N spin orbitals,

$$\phi_{SD} = \frac{1}{\sqrt{N!}} \begin{vmatrix} \phi_1(1) & \phi_2(1) & . & . & . & \phi_N(1) \\ \phi_1(2) & \phi_2(2) & . & . & . & \phi_N(2) \\ . & . & . & & & . \\ . & . & & . & & . \\ . & . & & & . & . \\ \phi_1(N) & \phi_2(N) & . & . & . & \phi_N(N) \end{vmatrix}$$

Here, ϕ_i is the molecular orbitals and orthogonality relation is

$$< \phi_i|\phi_j >= \delta_{ij} \tag{A.12}$$

Now we are ready to solve Electronic Hamiltonian,

$$H_e = \frac{-1}{2}{\nabla_i}^2 - \sum_{a}^{N_{nuclei}} \sum_{i}^{N_{el}} \frac{Z_a}{|R_a - r_i|} - \sum_{i}^{N_{el}} \sum_{j>i}^{N_{el}} \frac{1}{|r_i - r_j|} + \sum_{a}^{N_{nuclei}} \sum_{b>a}^{N_{nuclei}} \frac{Z_a Z_b}{|R_a - R_b|} \tag{A.13}$$

Define single particle operator h_i and two particle operator g_{ij} as follows,

$$h_i = \frac{-1}{2}{\nabla_i}^2 - \sum_{a}^{N_{nuclei}} \sum_{i}^{N_{el}} \frac{Z_a}{|R_a - r_i|} \tag{A.14}$$

$$g_{ij} = \frac{1}{|r_i - r_j|} \tag{A.15}$$

Energy of the Electronic Hamiltonian became

$$E = \sum_{i}^{Nel} h_i + \frac{1}{2} \sum_{i \neq j}^{N_{el}} (J_{ij} - K_{ij}) + Vnn \tag{A.16}$$

Here, J_j is coulomb operator and K_j is exchange operator and they defined as following in addition V_{nn} is taking constant here because of the Born-Oppenheimer approximation [41].

$$J_{ij} =< \phi_i(1)\phi_j(2)|g_{12}|\phi_i(1)\phi_j(2) > \tag{A.17}$$

$$K_{ij} =< \phi_i(1)\phi_j(2)|g_{12}|\phi_j(1)\phi_i(2) > \tag{A.18}$$

and definition of Fock operator is

$$F = h_i + \sum_j (J_j - K_j) \tag{A.19}$$

Now we are ready to get Hartree-Fock Equation and energy with Lagrange's Method of undetermined Multipliers.

A.2.1. Lagrange's Method of Multipliers

We are going to get the Hartree-Fock Equation by using Lagrange's Method of Multipliers. In this section, we take definitions from [17]. Firstly, we need to minimize Hartree-Fock energy with respect to changes in the molecular orbitals also we assume that orthonormality of the molecular orbitals remain unchanged after minimization of the energy.

$$\mathcal{L}[\phi_i] = E_{HF}[\phi_i] - \sum_{ij} \varepsilon_{ij}(< i|j > -\delta_{ij}) \tag{A.20}$$

here ε_{ij} is the undermined Lagrange multipliers and $< i|j >$ is the overlap between spin orbitals i and j definition of this as follows,

$$< i|j >= \int \phi_i{}^*(x)\phi_j(x)dx \tag{A.21}$$

Variational principle leads to $\delta\mathcal{L} = 0$ from here with using previous definition we can find Hartree-Fock equation,

$$F\phi_i = \varepsilon_i\phi_i \tag{A.22}$$

where F is the fock operator, ϕ is the molecular orbitals and ε is the eigenvalue of the fock operator.

In manybody systems, calculation of the coulomb integrals and exchange integrals are very hard computationally with molecular orbitals because of that we have to transform molecular orbitals into the basis set notation,

$$\phi_i = \sum_{\mu=1}^{N} C_{\mu i} \tilde{\phi}_\mu \tag{A.23}$$

Here $\tilde{\phi}_\mu$ is the atomic orbitals basis function, $C_{\mu i}$ is the coefficient number of for each i molecular orbitals and N is the total basis function number. If we put the ϕ_i into the eigenvalue equation of the Fock operator we will get,

$$\boldsymbol{FC} = \boldsymbol{SC\varepsilon} \tag{A.24}$$

in matrix notation. Here ε is the diagonal matrix of the orbital energies ε_i, S is the overlap matrix, C is the transformation coefficients matrix from molecular orbital to atomic orbitals finally F is the fock matrix.

APPENDIX B

THE BACKGROUND OF DENSITY FUNCTIONAL THEORY

B.1. Density Functional Theory

Solving Electronic Hamiltonian is the main goal of DFT but we are using different approach for solving this problem when we compare Hartree-Fock Theory. Foundation of DFT is Hohenberg and Kohn Theory and this theory states that the ground state electronic energy is determined completely by the electron density ρ [22].

B.1.1. The Hohenberg-Kohn Theorems

We see that Electronic Hamiltonian has three part; Kinetic energy T_e, attraction between nuclei and electrons V_{ne}, and electron-electron interaction V_{ee}. (Here we used Born-Oppenheimer approximation which states that Nuclei-Nuclei interaction is constant for large systems [41].) If we merge together this with Hohenberg Kohn theory,

$$H_{el} = T_e + V_{ee} + V_{ne} \tag{B.1}$$

and from this energy of the system can be defined as,

$$E[\rho(r)] = T_e[\rho(r)] + E_{ee}[\rho(r)] + E_{ne}[\rho(r)]. \tag{B.2}$$

Definition of $E_{ne}[\rho(r)]$ is

$$E_{ne}[\rho(r)] = -\sum_{i}^{N_{nuclei}} \int \frac{Z_a \rho(r)}{|R_a - r|} dr. \tag{B.3}$$

We can think electron electron interaction energy $E_{ee}[\rho(r)]$ as coulmb repulsion energy $J[\rho(r)]$ in Hartree-Fock equations without exchange part with definition,

$$J[\rho(r)] = \frac{1}{2} \int \int \frac{\rho(r)\rho(r')}{|r - r'|} dr dr' \tag{B.4}$$

Now we are ready to get into the Kohn-Sham equation.

B.1.2. Kohn-Sham Equation

First of all Kohn and Sham assumes that Hamiltonian of a system depend on the value of the interaction parameter λ with $0 \leq \lambda \leq 1$ [23].

$$H_\lambda = T + V_{ext}(\lambda) + \lambda V_{ee} \tag{B.5}$$

The external potential V_{ext} is equal to V_{ne} for $\lambda = 1$ (refer to fully interacting electrons of the system or real system) and $\lambda = 0$ case (refer to non-interacting electrons of the system) is Hartree-Fock case. From that approach Kohn and Sham states that if we divide kinetic energy into two part interacting and noninteracting part, non-interacting part of kinetic energy can be think like HF sense then one could just use Hartree-Fock expression for kinetic energy employing orbitals [16, 23]. This approximation leads to definition of the kinetic energy of non-interacting electrons as,

$$T_s = \sum_{i}^{N} < \phi_i | \frac{-1}{2} \nabla^2 | \phi_i > \tag{B.6}$$

and definition of density is as follows,

$$\rho(r) \quad = \quad \sum_{i}^{N} |\phi_i(r)|^2 \tag{B.7}$$

for a now there is no introduction of any exchange operator like in Hartree-Fock sense. After defnition of Exchange Correlation energy are going to handle this problem. Let's rewrite (B.2) with all these definitions

$$E_{DFT}[\rho(r)] = T_s[\rho(r)] + E_{ne}[\rho(r)] + J[\rho(r)] + E_{xc}[\rho(r)] \tag{B.8}$$

where E_{xc} is Exchange correlation energy and it includes kinetic energy term for interacting electrons and symetrization term for electrons. Because we divide kinetic energy into two parts interacting and non-interacting (correlating) part of kinetic energy. We put non-interacting kinetic energy into equation(B.8) and interacting kinetic energy part into the exchange correlation energy term. In addition we didn't introduce anywhere in our equations pauli principle so we have to put symmetrization term into exchange correlation energy term [16]. Now we are ready to define exchange correlation energy as

$$E_{xc}[\rho(r)] = (T_{exact}[\rho(r)] - T_s[\rho(r)]) + (E_{ee}[\rho(r)] - J[\rho(r)]) \tag{B.9}$$

From now on our main purpose is to find good excahange correlation energy to describe our system.

B.2. Natural Atomic Orbitals

The analysis of natural atomic orbital (NAO) and natural bond orbital (NBO) have been developed by Weinhold and coworkers to define the shape of atomic orbitals in the molecule, and to derive molecular bonds from electron density between atoms [9, 43]. According to NAO procedure, nonorthogonal AOs $\{\phi_i\}$ are transformed to corresponding

orthogonal AOs $\{\tilde{\phi}_i\}$ by the occupancy-weighted symmetric orthogonalization (OWSO) procedure

$$T_{OWSO}\{\phi_i\} = \{\tilde{\phi}_i\} \ , \ \langle\tilde{\phi}_i|\tilde{\phi}_j\rangle = \delta_{ij} \tag{B.10}$$

Here, the transformation matrix T_{OWSO} has the mathematical property of minimizing the occupancy-weighted, and has the mean-squared deviations of the nonorthogonal ϕ_i and the orthogonal $\tilde{\phi}_i$

$$min\Big\{\sum_i w_i \int |\tilde{\phi}_i - \phi_i|^2 d\tau\Big\}. \tag{B.11}$$

where weighting factor w_i is defined as

$$w_i = \langle\phi_i|\hat{\Gamma}|\phi_i\rangle. \tag{B.12}$$

Eq.(B.12) is taken as the occupancy of nonorthogonal ϕ_i and $\hat{\Gamma}$ is defined as diagonal expectation value of the density operator.

APPENDIX C

HIRSCH-FYE QUANTUM MONTE CARLO TECHNIQUE

In this section, the Hirsch-Fye Quantum Monte Carlo (HFQMC) algorithm for the multi-orbital Anderson model is described. This algorithm uses the Hubbard-Stratonovich (HS) transformation to convert the interacting electron system to a non-interacting one. Moreover, with the HS transformation, electrons move in a fluctuating magnetic field which is defined by a random set of spin configurations. These configurations are accepted or rejected by Monte Carlo (MC) algorithms such as the heat-bath algorithm or the Metropolis algorithm. In this way, the finite temperature Green's functions which measure the electronic and magnetic properties of the system are calculated.

The Hirsch-Fye QMC algorithm for the multi-orbital Anderson model is used in this study and with permision we use same algorithm in [25]. We have $5\ d$ orbitals and the size of the impurity Green's functions is $5\,L \times 5\,L$.

C.1. Hamiltonian of the System

Here the Hamiltonian for the multi-orbital case is defined :

$$H = \sum_{m\,\sigma} (\varepsilon_m - \mu)\, c^{\dagger}_{m\,\sigma}\, c_{m\,\sigma} + \sum_{m\,\sigma} \sum_{\nu=1}^{5} V_{m\,\nu}\, (c^{\dagger}_{m\,\sigma}\, d_{\nu\,\sigma} + h.c.) + \sum_{\nu=1}^{5} \sum_{\sigma} (\varepsilon_\nu - \mu)\, n_{\nu\,\sigma} + \sum_{\nu=1}^{5} U\, n_{\nu\uparrow}\, n_{\nu\downarrow}. \tag{C.1}$$

In the Anderson Hamiltonian of Ruthenium dye molecules, m denotes the host eigenstates which are obtained by density functional theory calculation and Hartree-Fock Theory calculations. Furthermore, ν is the index of the d orbitals ranging from 1 to 5. The Hamiltonian is divided into two parts which are the non-interacting part H_0 and the interacting part H_1

$$H \;\equiv\; H_0 + H_1, \tag{C.2}$$

where

$$H_0 = \sum_{m\,\sigma} (\varepsilon_m - \mu)\, c^{\dagger}_{m\,\sigma}\, c_{m\,\sigma} + \sum_{m\,\sigma} \sum_{\nu=1}^{5} V_{m\,\nu}\, (c^{\dagger}_{m\,\sigma}\, d_{\nu\,\sigma} + h.c.)$$
$$+ \sum_{\nu=1}^{5} \sum_{\sigma} (\varepsilon_\nu - \mu)\, n_{\nu\,\sigma} + \sum_{\nu=1}^{5} U/2\, (n_{\nu\uparrow} + n_{\nu\downarrow}), \tag{C.3}$$

$$H_1 = \sum_{\nu=1}^{5} U n_{\nu\uparrow} n_{\nu\downarrow} - \sum_{\nu=1}^{5} U/2\, (n_{\nu\uparrow} + n_{\nu\downarrow}). \tag{C.4}$$

and the interaction Hamiltonian H_1 is treated by using the Hubbard-Stratonovich transformation.

C.2. The Hubbard-Stratonovich Transformation, Trotter Break-Up and Partition Function

The next step is the Hubbard-Stratonovich (HS) transformation. In the interaction Hamiltonian, if we replace $n_{d\,\nu\uparrow}\, n_{d\,\nu\downarrow}$ term with

$$n_{\nu\uparrow}\, n_{\nu\downarrow} = -\frac{1}{2}\, (n_{\nu\uparrow} - n_{\nu\downarrow})^2 + \frac{1}{2}\, (n_{\nu\uparrow} + n_{\nu\downarrow}), \tag{C.5}$$

we obtain

$$H_1 = \sum_{\nu} -\frac{U}{2}\, (n_{\nu\uparrow} - n_{\nu\downarrow})^2. \tag{C.6}$$

With $\cosh(\lambda_\nu) = e^{\frac{1}{2}\Delta\tau U}$,

$$exp\ \{-\Delta\tau\, H_1\} \;=\; exp\left\{-\Delta\tau \sum_{\nu} \frac{U}{2}\, (n_{\nu\uparrow} - n_{\nu\downarrow})^2\right\} \tag{C.7}$$

$$\;=\; \frac{1}{2} \sum_{S_{l\nu}\,=\,\pm 1} exp\left\{\sum_{\nu} \lambda_\nu\, S_{l\nu}\, (n_{\nu\uparrow} - n_{\nu\downarrow})\right\}, \tag{C.8}$$

where $S_{l\nu}$ is the auxiliary Hubbard-Stratonovich field. The partition function is

$$Z = Tr\ \left[e^{-\beta\, H}\right]. \tag{C.9}$$

By taking small time step in imaginary time with $\Delta\tau\, L = \beta$, we do the Trotter approximation

$$e^{-\Delta\tau\,(H_0+H_1)} = e^{-\Delta\tau\, H_0}\, e^{-\Delta\tau\, H_1} + \theta\,(\Delta\tau^2[H_0, H_1]). \tag{C.10}$$

The partition function is rewritten:

$$\begin{aligned} Z &= Tr\ \left[e^{-\beta\, H}\right] && \text{(C.11)}\\ &= Tr\ \left[\prod_{l=1}^{L} e^{-\Delta\tau\,(H_0+H_1)}\right] && \text{(C.12)}\\ &\simeq Tr\ \left[\prod_{l=1}^{L} e^{-\Delta\tau\, H_0}\, e^{-\Delta\tau\, H_1} + \theta\,(\Delta\tau^2)\right]. && \text{(C.13)} \end{aligned}$$

By using the Hubbard-Stratonovich transformation and the Trotter approximation, we write the partition function.

$$\begin{aligned} Z &= Tr\ \left[\prod_{l=1}^{L} exp\ \{-\Delta\tau\, H_0\}\ \times\ exp\ \{-\Delta\tau\, H_1)\}\right]\\ =& Tr \prod_{l=1}^{L} \frac{1}{2} \sum_{S_{l\nu}=\pm 1} exp\left\{-\Delta\tau \sum_{i\,j} a^{\dagger}_{i\uparrow}\, K_{i\,j}\, a_{j\uparrow}\right\} exp\left\{\sum_{\nu} \lambda_\nu\, S_{l\,\nu}\, n_{d\,\nu\uparrow}\right\}\\ &\qquad \times exp\left\{-\Delta\tau \sum_{i\,j} a^{\dagger}_{i\downarrow}\, K_{i\,j}\, a_{j\downarrow}\right\} exp\left\{\sum_{\nu} -\lambda_\nu\, S_{l\,\nu}\, n_{d\,\nu\downarrow}\right\} && \text{(C.14)}\\ &= \frac{1}{2^{5L}}\, Tr \prod_{l=1}^{L} \sum_{S_{1\,\nu}, S_{2\,\nu}, \ldots, S_{L\,\nu}=\pm 1} exp\left\{-\Delta\tau\, H^{\uparrow}(l)\right\}\, exp\left\{-\Delta\tau\, H^{\downarrow}(l)\right\}, && \text{(C.15)} \end{aligned}$$

where

$$H_0 = \sum_{i,j,\sigma} a^{\dagger}_{i\,\sigma}\, K_{i\,j}\, a_{j\,\sigma} \tag{C.16}$$

$$H^{\uparrow}(l) = \sum_{i\,j} a^{\dagger}_{i\uparrow}\, K_{i\,j}\, a_{j\uparrow} - \frac{\sum_{\nu}\, \lambda_{\nu}\, S_{l\,\nu}\, n_{d\,\nu\uparrow}}{\Delta\tau} \tag{C.17}$$

$$H^{\downarrow}(l) = \sum_{i\,j} a^{\dagger}_{i\downarrow}\, K_{i\,j}\, a_{j\downarrow} + \frac{\sum_{\nu}\, \lambda_{\nu}\, S_{l\,\nu}\, n_{d\,\nu\downarrow}}{\Delta\tau}. \tag{C.18}$$

a denotes both c and d orbitals and now, we define for fixed l

$$V^{\sigma}_{\nu l} = \sigma\, \lambda_{\nu}\, S_{\nu}. \tag{C.19}$$

$V^{\sigma}_{\nu} = \sigma\, \lambda_{\nu}\, S_{\nu}\; |\nu\rangle\, \langle\nu|$ only acts at the impurity sites and the matrix form of $e^{V^{\sigma}_{\nu}}$ is

$$e^{V^{\sigma}_{\nu}} = \begin{bmatrix} e^{\sigma\,\lambda_{\nu=1}\,S_{\nu=1}} & & & & & & & & \\ & e^{\sigma\,\lambda_2\,S_2} & & & & & & 0 & \\ & & e^{\sigma\,\lambda_3\,S_3} & & & & & & \\ & & & e^{\sigma\,\lambda_4\,S_4} & & & & & \\ & & & & e^{\sigma\,\lambda_5\,S_5} & & & & \\ & & & & & & 1 & & \\ & 0 & & & & & & \ddots & \\ & & & & & & & & 1 \end{bmatrix}$$

This is a diagonal $(N+5)\times(N+5)$ matrix. In this matrix, diagonals are $e^{\sigma\,\lambda_{\nu}\,S_{\nu}}$ for the impurity sites and 1 for the host sites and we represent it with

$$e^{V_\nu^\sigma} = \begin{bmatrix} \bullet & & & & & & & \\ & \bullet & & & & & & \\ & & \bullet & & & & 0 & \\ & & & \bullet & & & & \\ & & & & \bullet & & & \\ & & & & & 1 & & \\ & & & & & & 1 & \\ & & 0 & & & & & \ddots \\ & & & & & & & & \ddots \\ & & & & & & & & & 1 \end{bmatrix}$$

Let's introduce now the following matrix $B_{l\nu}^\sigma = e^{-\Delta\tau\, K}\, e^{V_{l\nu}^\sigma}$. By using this definition, we can write the partition function

$$Z = \sum_{S_{1\nu}, S_{2\nu} \ldots . = \pm 1} \prod_{\sigma = \pm 1} det[I + B_{L\,\nu}(\sigma)\, B_{L-1\,\nu}(\sigma) \ldots . B_{1\,\nu}(\sigma)] \qquad \text{(C.20)}$$

$$\equiv \sum_{S_{1\,\nu}, S_{2\,\nu} \ldots . = \pm 1} det\, \vartheta_{S_{1\,\nu}\, S_{2\,\nu} \ldots . . S_{L\,\nu}}(\uparrow)\, det\, \vartheta_{S_{1\,\nu} S_{2\,\nu} \ldots . . S_{L\,\nu}}(\downarrow) \qquad \text{(C.21)}$$

$\vartheta_\nu(\sigma)$ is an $(N+5)\,L \times (N+5)\,L$ matrix, where K is a $(N+5) \times (N+5)$ matrix for the bilinear part of the H and N is the number of the host states. Furthermore, the matrix representation of $e^{V_{l\nu}^\sigma}$ is

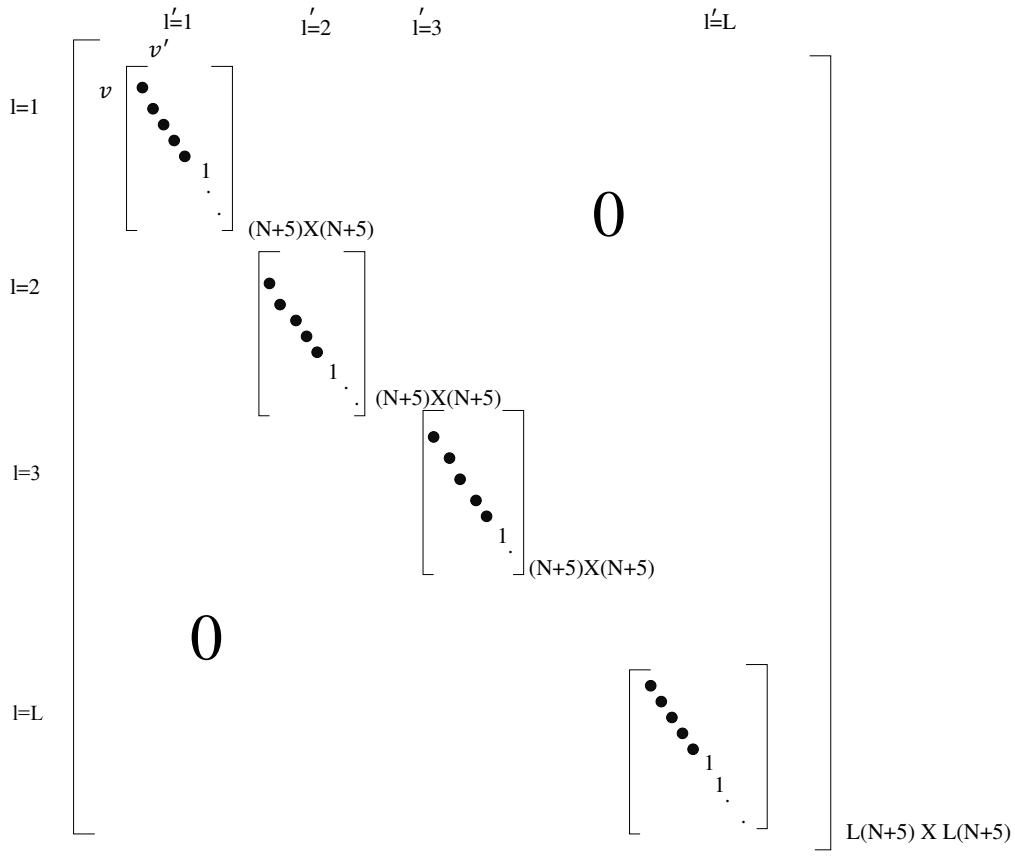

In this matrix, d orbitals are shown with the bullets and the host states are 1. Moreover, the matrix elements at the $l \neq l'$ and $\nu \neq \nu'$ are zero.

C.3. Dyson's Equation for the Green's Functions

We define the single particle Green's function as

$$G^{\sigma}_{\nu\,\nu'} = -\left\langle T_\tau d_{\nu\,\sigma}\, d^{\dagger}_{\nu'\,\sigma}\right\rangle \tag{C.22}$$

$$= \frac{-Tr\, T_\tau\, e^{-\beta\, H} d_{\nu\,\sigma}(l)\, d^{\dagger}_{\nu'\,\sigma}(l')}{Tr\, e^{-\beta\, H}}. \tag{C.23}$$

The relation between the $\vartheta_\nu(\sigma)$ and the Green's function by the identity

$$G^{\sigma}_{\nu\,\nu'} = (\vartheta_\nu(\sigma))^{-1}. \tag{C.24}$$

as shown in [44]. The size of the $\vartheta_{S_1,S_2,...,S_L}$ is $(N+5)\,L \times (N+5)\,L$ and the calculation of the Green's functions for every set $S_1, S_2, ..., S_L$ of spins from this large size matrix is very difficult.

Hirsch and Fye [39] noted that the Green's function G can be calculated only once for a certain spin configuration $S_1, S_2, ..., S_L$ and after that, G can be updated for a new set of configuration where only one spin is changed. The Green's functions which are different only by one "spin flip" are related to each other by a Dyson's equation.

The new configuration Green's function $G^{'}_{\nu\,\nu'}$ and the old configuration Green's function $G_{\nu\,\nu'}$ are related to each other by a Dyson's equation (by omitting σ)

$$G^{'}_{\nu\,\nu'} = G_{\nu\,\nu'} + (G_{\nu\,\nu'} - I)\,(e^{V^{'}_{\nu} - V_{\nu}} - I)\,G^{'}_{\nu\,\nu'} \tag{C.25}$$

C.4. Impurity Green's Function for the New Hubbard-Stratonovich Field Configuration

After the spin $S_{l\,\nu}$ is flipped, the new impurity Green's function is obtained from the relation

$$G^{'}_{\nu\,\nu'} = G_{\nu\,\nu'} + (G_{\nu\,\nu'} - I)\,(e^{V^{'}_{l\nu} - V_{l\nu}} - I)\,G^{'}_{\nu\,\nu'}. \tag{C.26}$$

By substituting

$$G^{'}_{\nu\,\nu'} = [I - (G_{\nu\,\nu'} - I)\,((e^{V^{'}_{l\nu} - V_{l\nu}} - I)]^{-1}\,G_{\nu\,\nu'}, \tag{C.27}$$

we have

$$\begin{aligned} G^{'}_{\nu\,\nu'} \;\; = \;\; & G_{\nu\,\nu'} + (G_{\nu\,\nu'} - I)\,(e^{V^{'}_{l\nu} - V_{l\nu}} - I) \\ & \times [I - (G_{\nu\,\nu'} - I)(e^{V^{'}_{l\nu} - V_{l\nu}} - I)]^{-1}\,G_{\nu\,\nu'}. \end{aligned} \tag{C.28}$$

We define

$$A = I + (I - G_{\nu\,\nu'})\,(e^{V'_{l\nu} - V_{l\nu}} - I). \tag{C.29}$$

After $S_{l\,\nu}$ is flipped, the new impurity Green's function is given by

$$\begin{aligned} G'_{\nu\,\nu'}(l_1,\, l_2) &= G_{\nu\,\nu'}(l_1, l_2) \\ &+ \sum_{l_3, l_4} (G_{\nu\,\nu'} - I)_{l_1, l_3}\,(e^{V'_{l\nu} - V_{l\nu}})_{l_3,\, l_3}\,(A^{-1})_{l_3,\, l_4}\,(G_{\nu\,\nu'})_{l_4, l_2}. \end{aligned} \tag{C.30}$$

Hence

$$\begin{aligned} G'_{\nu\,\nu'}(l_1, l_2) &= G_{\nu\,\nu'}(l_1, l_2) \\ &+ \sum_{l_4} (G_{\nu\,\nu'}(l_1, l) - \delta_{l_1, l}\,\delta_{\nu,\,\nu'})\,(e^{V'_{l\nu} - V_{l\nu}})\,(A^{-1})_{l,\, l_4}\,(G_{\nu\,\nu'})_{l_4, l_2}. \end{aligned} \tag{C.31}$$

We define

$$\left(e^{V^{\sigma'}_{l'\,\nu'} - V^{\sigma}_{l\,\nu}} \right) = \delta_{\nu\,\nu'}\,\delta_{l\,l'}\,e^{\sigma\,\lambda_\nu\,(\,S_{l'\,\nu'} - S_{l\,\nu})} \tag{C.32}$$

so

$$(A^{-1})_{l,\, l_4; \nu,\, \nu'} = \delta_{l\,l_4}\,\delta_{\nu\,\nu'}\,\frac{1}{[I + (I - G_{\nu\,\nu'}(l,l))(e^{(V'_{l\nu} - V_{l\nu})} - I)]}. \tag{C.33}$$

Hence

$$\begin{aligned} G'_{\nu\,\nu'}(l_1,\, l_2) &= G_{\nu\,\nu'}(l_1,\, l_2) + (G_{\nu\,\nu'}(l_1,\, l) - \delta_{l_1, l}\,\delta_{\nu\,\nu'})(e^{V'_\nu - V_\nu} - I) \\ &\times \frac{1}{[I + (I - G_{\nu\,\nu'}(l,l))(e^{V'_{l\,\nu} - V_{l\,\nu}} - I)]}\,G_{\nu\,\nu'}(l,\, l_2) \end{aligned} \tag{C.34}$$

C.5. Ratio of the Fermion Determinants

For a proposed change of the HS field $S_{l\,\nu}$,

$$S_{l\,\nu} \rightarrow S^{'}_{l\,\nu} = -S_{l\,\nu} \tag{C.35}$$

The probability of acceptence of the new configuration is proportional to the ratio of determinants of the new and old configuration.

$$R_{\nu\,\sigma} = \frac{det\,\vartheta_{S^{'}_{l\,\nu}}(\sigma)}{det\,\vartheta_{S_{l\,\nu}}(\sigma)} = I + [I - G^{\sigma}_{\nu\,\nu'}(l,l)]\,(e^{V^{\sigma}_{l\nu}{}^{'} - V^{\sigma}_{l\nu}} - I). \tag{C.36}$$

In order to prove this, we start from

$$\tilde{G}^{'}_{\nu\,\nu'} = \tilde{G}_{\nu\,\nu'} - \tilde{G}_{\nu\,\nu'}\,(e^{-V^{'}_{l\nu}} - e^{-V_{l\nu}})\,\tilde{G}^{'}_{\nu\,\nu'}, \tag{C.37}$$

where

$$\tilde{G}_{\nu\,\nu'} = e^{V_{l\nu}}\,G_{\nu\,\nu'}. \tag{C.38}$$

Multiplying both sides with $(\tilde{G}^{'}_{\nu\,\nu'})^{-1}$ on the right, we get

$$I = \tilde{G}_{\nu\,\nu'}\,(\tilde{G}^{'}_{\nu\,\nu'})^{-1} - \tilde{G}_{\nu\,\nu'}\,(e^{-V^{'}_{l\nu}} - e^{-V_{l\nu}}). \tag{C.39}$$

Hence

$$\tilde{G}_{\nu\,\nu'}\,(\tilde{G}^{'}_{\nu\,\nu'})^{-1} = I + \tilde{G}_{\nu\,\nu'}\,(e^{-V^{'}_{l\nu}} - e^{-V_{l\nu}}). \tag{C.40}$$

Since

$$\tilde{G}_{\nu\,\nu'} = e^{V_{l\nu}}\, G_{\nu\,\nu'} = e^{V_{l\nu}}\, \vartheta_{l\nu}^{-1}, \tag{C.41}$$

we have

$$\begin{aligned} (e^{V_\nu}\, \vartheta_{l\nu}^{-1})\, \left[e^{V_{l\nu}^{'}}\, (\vartheta_{l\nu}^{'})^{-1}\right]^{-1} &= I + e^{V_{l\nu}}\, G_{\nu\,\nu'}\, (e^{-V_{l\nu}^{'}} - e^{-V_{l\nu}}), & \text{(C.42)} \\ e^{V_{l\nu}}\, (\vartheta_{l\nu}^{-1}\, \vartheta_{l\nu}^{'})\, e^{-V_{l\nu}^{'}} &= I + e^{V_{l\nu}}\, G_{\nu\,\nu'}\, (e^{-V_{l\nu}^{'}} - e^{-V_{l\nu}}). & \text{(C.43)} \end{aligned}$$

Here, we multiply on the left with $e^{-V_{l\nu}}$ and on the right with $e^{V_{l\nu}^{'}}$,

$$\begin{aligned} \vartheta_{l\nu}^{-1}\, \vartheta_{l\nu}^{'} &= e^{-V_{l\nu}}\, e^{V_{l\nu}^{'}} + G_{\nu\,\nu'}\, (e^{-V_{l\nu}^{'}} - e^{-V_{l\nu}})\, e^{V_{l\nu}^{'}} & \text{(C.44)} \\ \vartheta_{l\nu}^{-1}\, \vartheta_{l\nu}^{'} &= e^{V_{l\nu}^{'} - V} + G_{\nu\,\nu'}\, (I - e^{V_{l\nu}^{'} - V_{l\nu}}) & \text{(C.45)} \\ &= e^{V_{l\nu}^{'} - V_{l\nu}} + (G_{\nu\,\nu'} - I)(I - e^{V_{l\nu}^{'} - V_{l\nu}}) + I\, (I - e^{V_{l\nu}^{'} - V_{l\nu}}). & \text{(C.46)} \end{aligned}$$

Hence

$$\vartheta_{l\nu}^{-1}\, \vartheta_{l\nu}^{'} = I + (I - G_{\nu\,\nu'})(e^{V_{l\nu}^{'} - V_{l\nu}} - I). \tag{C.47}$$

By taking the determinant of the both sides, we obtain

$$\frac{det\, \vartheta_{l\nu}^{'}}{det\, \vartheta_{l\nu}} = \det\, (I + (I - G_{\nu\,\nu'})\, (e^{V_{l\nu}^{'} - V_{l\nu}} - I)) \tag{C.48}$$

$(e^{V_{l\nu}^{'} - V_{l\nu}} - I)$ has the non-zero elements only at the d sites so $I + (I - G_{\nu\,\nu'})(e^{V_{l\nu}^{'} - V_{l\nu}} - I)$ has the form

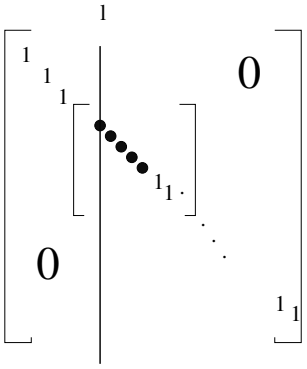

In this matrix, the bullets show the impurity sites and the line denotes a single flip at an arbitrary l and ν orbital. This way

$$\det\Big(I+(I-G_{\nu\,\nu'})(e^{V'_{l\nu}-V_{l\nu}}-I)\Big)=I+(I-G^{\sigma}_{\nu\,\nu'}(l,l))(e^{V'_{l\nu}-V_{l\nu}}-I). \quad \text{(C.49)}$$

Hence

$$R_{\nu\,\sigma}=I+(I-G^{\sigma}_{\nu\,\nu'}(l,l))(e^{V'_{l\nu}-V_{l\nu}}-I). \quad \text{(C.50)}$$

In heat-bath method, the transition probability from one state $S_{l\,\nu}$ to another state $S'_{l\,\nu}$ is

$$P(S_{l\,\nu}\ \rightarrow\ S'_{l\,\nu})=\frac{1}{\prod_{\nu\,\sigma}\ R_{\nu\,\sigma}\ +\ 1} \quad \text{(C.51)}$$

Then, by random number generator, if

$$P > \text{random number} \longrightarrow \text{accept}$$

else reject.

C.6. Impurity Green's Functions for the Multi-Orbital Case for When the Hubbard-Stratonovich Field is Zero

The impurity and host Green's functions with no hybridization and no Coulomb interaction are given by

$$G^{00}_{\nu\,\nu'} = \frac{\delta_{\nu\,\nu'}}{i\omega_n - (\epsilon_{d\,\nu} - \mu)} \qquad \text{and} \qquad G^{00}_{m}(i\omega_n) = \frac{1}{i\omega_n - (\varepsilon_m - \mu)}. \tag{C.52}$$

The Green's function with hybridization and no Coulomb interaction can be evaluated by using the following diagrams

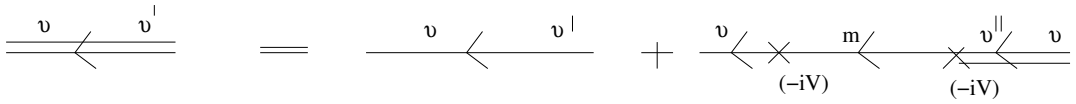

Figure C.1. Feynman diagram representing the impurity Green's function $G^0_{\nu\,\nu'}(i\,\omega_n)$ for the $U = 0$. The double lines denote $G^0_{\nu\,\nu'}(i\,\omega_n)$ while the single lines denote $G^{00}_{m}(i\,\omega_n)$ and $G^{00}_{\nu}(i\,\omega_n)$, respectively.

$$\begin{aligned} G^0_{\nu\,\nu'}(i\omega_n) \;\; &= \;\; G^{00}_{\nu\,\nu'}(i\omega_n) + \sum_{\nu''} G^{00}_{\nu\,\nu'}(i\,\omega_n) \\ &\qquad \times \left\{ \sum_m V_{\nu m}\, V_{m\nu''}\, G^{00}_m(i\,\omega_n) \right\} G^0_{\nu''\,\nu'}(i\omega_n) \end{aligned} \tag{C.53}$$

and let's define the self-energy

$$F_{\nu\,\nu''}(i\omega_n) \;\equiv\; \sum_m V_{m\nu}\, V_{\nu'' m}\, \frac{1}{i\omega_n - (\varepsilon_m - \mu)}. \tag{C.54}$$

Then;

$$G^0_{\nu\,\nu'}(i\,\omega_n) = G^{00}_{\nu\,\nu'}(i\omega_n) + G^{00}_{\nu\,\nu'}(i\,\omega_n) \sum_{\nu''} F_{\nu\,\nu''}(i\omega_n)\, G^0_{\nu''\,\nu'}(i\omega_n), \tag{C.55}$$

$$G^0_{\nu\,\nu'}(i\omega_n) = G^{00}_{\nu\,\nu'}\left\{\underbrace{1+\sum_{\nu''} F_{\nu\,\nu''}(i\omega_n)\,G^0_{\nu''\,\nu'}(i\omega_n)}_{T_{\nu\,\nu'}(i\omega_n)}\right\}. \tag{C.56}$$

$$T_{\nu\,\nu'}(i\omega_n) = 1+\sum_{\nu''} F_{\nu\,\nu''}(i\omega_n)\,G^0_{\nu''\,\nu'}(i\omega_n). \tag{C.57}$$

$$\sum_{\nu''} T_{\nu\,\nu''}(i\,\omega_n)\,G^0_{\nu''\,\nu'}(i\,\omega_n) = G^{00}_{\nu}(i\,\omega_n). \tag{C.58}$$

So

$$G^0_{\nu\,\nu'}(i\,\omega_n) = \sum_{\nu''} T^{-1}_{\nu\,\nu''}(i\,\omega_n)\,G^{00}_{\nu''}(i\,\omega_n) \tag{C.59}$$

Up to now, we have got $i\omega_n$ dependent Green's functions. Now, all Green's functions are transformed to imaginary time space to be used in the Hirsch-Fye algorithm. Here, $G^0(l,l^{'})$ is defined by

$$G^0_{\nu\,\nu'}(l,l^{'}) = T\sum_{iw_n} e^{-iw_n\,\Delta\tau(l-l^{'})}\,G^0_{\nu\,\nu'}(iw_n) \tag{C.60}$$

for $l,l^{'}=1,.....,L$. However, for $l=l^{'}$ cases, attention is required for implementation of boundary conditions in τ_l space. For $l=l^{'}$, we define $G^0_{\nu\,\nu'}(l,l)$

$$G^0_{\nu\,\nu'}(l,l) = \lim_{\tau\,\to\,0^+} T\sum_{iw_n} e^{-i\,\omega_n\,\tau} G^0_{\nu\,\nu'}(i\,\omega_n). \tag{C.61}$$

Our choice for $l = l^{'}$ gives,

$$G^{0}_{\nu\,\nu'}(l,l) = -\left\langle T_{\tau}\, c_{\nu}(\tau_l)\, c^{\dagger}_{\nu'}(\tau_l)\right\rangle_0 \tag{C.62}$$

$$= -[1 - \left\langle c_{\nu}(\tau_l)\, c^{\dagger}_{\nu'}(\tau_l)\right\rangle_0] \tag{C.63}$$

$$= -[1 - \langle n_{d\,\nu\,\sigma}\rangle_0]. \tag{C.64}$$

In the program, we calculate $G^{0}_{\nu\,\nu'}(l,l')$ for $l \neq l'$ and $l, l' = 1, ..., L$ cases. After that, we use

$$G^{0}_{\nu\,\nu'}(\tau_l) = -G^{0}_{\nu\,\nu'}(\tau_l + \beta) = -G^{0}_{\nu\,\nu'}(\tau_{l+L}) \tag{C.65}$$

to obtain $G^{0}_{\nu\,\nu'}(\tau_l)$ for $-L \leq l \leq -1$ and $l = L$.

C.7. Procedure to Update Impurity Green's Functions

Procedure to update Green's functions is Firstly, calculate the $G^{0}_{\nu\,\nu'}(i\,\omega_n)$ which is the Green's function for non-zero hybridization and no Hubbard field. After that, for an initial spin configuration, $G_{\nu\,\nu'}(l,l')$ is calculated. State of whole system is changed from $S_{l\,\nu}$ to $S_{l\,\nu}{}'$ with probability $P(S_{l\,\nu} \rightarrow S'_{l\,\nu})$. Then the Green's function is updated if $P(S_{l\,\nu} \rightarrow S'_{l\,\nu})$ is larger than the random number which is generated from 1 to 0.

C.8. Flow chart for the HFQMC algorithm

- Calculate the non-interacting (HS field = 0) Green's function G^0.
- By random number generator, choose starting HS field configuration.
- Calculate the Green's function G from the below equation,

$$G^{\sigma}_{\nu\nu'} = [I + (G^{0}_{\nu\nu'} - I)(I - e^{V^{\sigma}_{\nu l}})]^{-1} G^{0}_{\nu\nu'} \tag{C.66}$$

- Choose imaginary time slice and $3d$ orbital randomly for spin flip and accept or

reject the spin flip with respect to heat-bath QMC algorithm.

- Calculate the new Green's function $G'_{\nu\nu'}$ by using Dyson's equation.

$$G'_{\nu\,\nu'}(l_1,\,l_2) = G_{\nu\,\nu'}(l_1,\,l_2) + (G_{\nu\,\nu'}(l_1,\,l) - \delta_{l_1,l}\,\delta_{\nu\,\nu'})(e^{V'_{l\nu}-V_{l\nu}} - I) \times \frac{1}{[I + (I - G_{\nu\,\nu'}(l,l))(e^{V'_{l\,\nu}-V_{l\,\nu}} - I)]}\, G_{\nu\,\nu'}(l,\,l_2) \tag{C.67}$$

- After certain number of warm up sweeps, the system reaches the equilibrium.
- Then, measurements start. In order to eliminate the correlations, a few update sweeps between the measurements should be considered.
- Finally, calculate the averages and standart deviation of the measurements.